Section 3 Optics and Devices

Chapter 1. Optics and Quantum Electronics

Academic and Research Staff

Professor Hermann A. Haus, Professor Erich P. Ippen, Professor James G. Fujimoto, Professor Peter L. Hagelstein, Dr. Brett E. Bouma, Dr. Joseph A. Izatt

Visiting Scientists and Research Affiliates

Dr. Mark E. Brezinski,[1] Dr. Charles P. Lin, Dr. Brent E. Little, Dr. Shu Namiki, Dr. Matasaka Shirasaki

Graduate Students

Laura E. Adams, Susan Bach, Keren Bergman, Igor P. Bilinsky, Luc Boivin, Stephen A. Boppart, Jerry C. Chen, Jay N. Damask, Ali M. Darwish, Christopher R. Doerr, David J. Dougherty, Siegfried B. Fleischer, Marc Fleury, Boris Golubovic, James G. Goodberlet, Michael R. Hee, Charles T. Hultgren, David J. Jones, Sumanth Kaushik, Mohammed J. Khan, Farzana I. Khatri, Gadi Lenz, Martin H. Muendel, John D. Moores, Lynn E. Nelson, Malini Ramaswamy-Paye, Timothy A. Savas, Chi-Kuang Sun, Kohichi R. Tamura, Guillermo J. Tearney, Constantine Tziligakis, Morrison Ulman, William S. Wong

Undergraduate Students

Leo Chun, Charles Yu

Technical and Support Staff

Mary C. Aldridge, Donna L. Gale, Cynthia Y. Kopf

1.1 Fiber Ring Lasers

Sponsors

Charles S. Draper Laboratories
Contract DL-H-467138
Joint Services Electronics Program
Contract DAAL03-92-C-0001
Grant DAAH04-95-1-0038
U.S. Air Force - Office of Scientific Research
Contract F49620-91-C-0091

Project Staff

Professor Hermann A. Haus, Professor Erich P. Ippen, Christopher R. Doerr, Lynn E. Nelson, Kohichi R. Tamura

Several new fiber ring laser systems have been developed over the past few years in the Optics and Devices Group of RLE. The simplicity of design of these systems allows for modifications that lead to outstanding performance characteristics.

The laser consists of an erbium doped fiber and an undoped fiber forming a ring. The net dispersion (group velocity as a function of frequency) can be adjusted through proper choice of the two fiber segments. Polarizers and quarter wave plates control the polarization of the mode circulating in the ring. The polarizers can be realized entirely with fiber components. An isolator assures propagation in one direction around the ring (see figure 1). By proper adjustment of the polarizers, the self-phase modulation of the two polarizations of the mode circulating in the ring is transformed into amplitude modulation such as to spontaneously form pulses in the ring by injection locking of the modes of the ring resonator (modelocking). Pulses are formed when higher intensities experience less loss than lower intensities. We call this mechanism additive pulse modelocking (APM), and this acronym is now accepted in the literature as the descriptor of this form of modelocking.[2] The ring delivers pulses of the order of 400 fs duration at the round-trip rate of 40 MHz. We have studied the wavelength tuning

---

[1] Massachusetts General Hospital, Boston, Massachusetts.

[2] H.A. Haus, E.P. Ippen, and K. Tamura, "Additive Pulse Modelocking in Fiber Lasers," *IEEE J. Quant. Electron.* 30: 200-208 (1994).

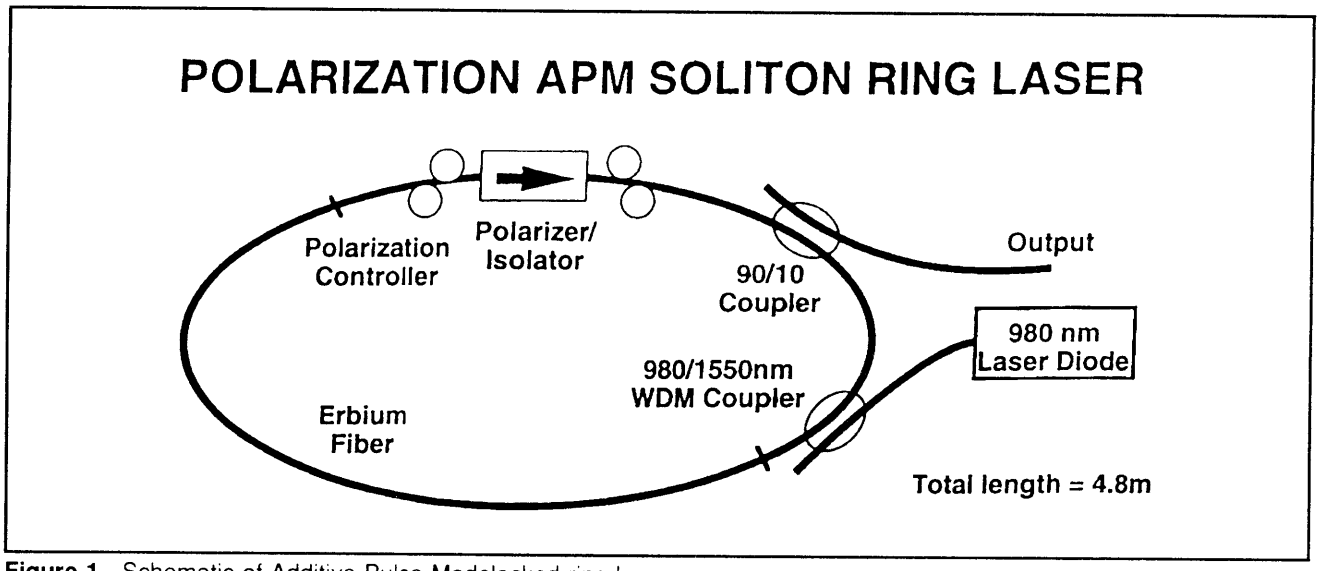

Figure 1. Schematic of Additive Pulse Modelocked ring laser.

and filtering characteristics of this laser[3] and developed optimization criteria.[4] Last year, with proper adjustment of the fiber dispersion, we were able to produce pulses as short as 69 fs.[5] The system has been copied by a group at Bell Laboratories for their use. We are currently in the process of working with Clark MXZ to commercialize these systems.

As mentioned in the introduction, the simplicity of the system permits modifications for the realization of different operating characteristics. For many purposes it is desirable to generate pulses at much higher rates than 40 MHz. This can be accomplished with a modulator in the ring, yet not without further precautions. Indeed, a modulator by itself produces pulse trains of very poor pulse-to-pulse stability, because the gain relaxation time is of the order of a millisecond, and there is no mechanism to regulate the energy from pulse to pulse. Last year, we reported operation of a harmonically modelocked system operating at 1 GHz, using a modified APM mechanism, used to stabilize the energy from pulse to pulse.[6] Instead of providing decreasing loss for increasing intensity, the APM mechanism was reversed by a change of the polarization controllers to limit peak intensities. In this way, we obtained stable pulse-streams at 1 GHz, the highest frequency accessible with our modulator. MIT Lincoln Laboratory has copied our system and, with their 20 GHz modulator, produced stable pulse streams at this much higher repetition rate.

The modelocked ring laser described above delivers pulses of width according to the formula for active modelocking, dictated by the magnitude of the modulator drive which is limited. In the 1 GHz system just described, the pulse widths are 15 ps. In an attempt to generate shorter pulses at a high repetition rate, Chris Doerr, a graduate student, discovered asynchronous modelocking, a new principle of modelocking fiber ring lasers.[7] A phase modulator is used instead of the amplitude modulator described before. The modelocking drive of 1 GHz is detuned by about 15 kHz from the frequency synchronous with a harmonic of the round-trip frequency. The pulses are now 1 ps long and

---

[3] K. Tamura, L.E. Nelson, H.A. Haus, and E.P. Ippen, "Soliton versus Non-soliton Operation of Fiber Ring Lasers," *Appl. Phys. Lett.* 62: 149-151 (1994); K. Tamura, C.R. Doerr, L. Nelson, H.A. Haus, and E.P. Ippen, "Technique for Obtaining High-energy Ultrashort Pulses from an Additive-pulse Mode-locked Erbium-doped Fiber Ring Laser," *Opt. Lett.* 19: 46-48 (1994); K. Tamura, C.R. Doerr, H.A. Haus, and E.P. Ippen, "Soliton Fiber Ring Laser Stabilization and Tuning with a Broad Intracavity Filter," *IEEE Photon. Technol. Lett.* 6: 697-699 (1994).

[4] K. Tamura, E.P. Ippen, and H.A. Haus, "Optimization of Filtering in Soliton Fiber Lasers," *Photon. Technol. Lett.* 6 (1994).

[5] H.A. Haus, K. Tamura, L.E. Nelson, and E.P. Ippen, "Stretched Pulse Additive Pulse Modelocking of Fiber Lasers," *IEEE J. Quant. Electron.* 31: 591-592 (1994).

[6] C.R. Doerr, H.A. Haus, E.P. Ippen, M. Shirasaki, and K. Tamura, "Additive-Pulse Limiting," *Opt. Lett.* 19: 31-33 (1994).

[7] C.R. Doerr, H.A. Haus, and E.P. Ippen, "Asynchronous Soliton Modelocking," *Opt. Lett.* 19: 1958-1960 (1994).

travel around the loop at their own rate. The modelocking drive serves the purpose of starting the system and of arranging the pulses equidistantly around the loop by refreshing the pulse stream every time it becomes synchronous with the modelocking drive. Because phase modulation is used, instead of amplitude modulation, the pulses do not experience modulator induced loss when they drift out of alignment with the modelocking drive. The APM action in the loop is responsible for the shortening of the pulse to 1 ps.

This is an entirely new principle of modelocking made possible by the pulse-forming capabilities of the fiber loop. The APM mechanism of the fiber loop provides the short pulse widths. The limiting of the APM mechanism provides the stability for the pulse-to-pulse energy. If any conventional modelocked system were detuned in the same way, modelocked operation would simply cease. We believe that this asynchronous modelocking principle is applicable to all systems with their own passive pulse-shaping mechanism (e.g., Kerr Lens Modelocking) if harmonic modelocking with short pulse widths is sought.

In the upcoming year, we shall explore the asynchronous modelocking principle for its potential use in optical storage rings (see section 1.2).

1.2 Fiber Storage Ring

Sponsors

Charles S. Draper Laboratories
Contract DL-H-467138
U.S. Air Force - Office of Scientific Research
Contract F49620-91-C-0091

Project Staff

Professor Hermann A. Haus, Professor Erich P. Ippen, Christopher R. Doerr, David J. Jones, John D. Moores, William S. Wong

In a theoretical paper published in 1992,[8] we proposed that a fiber loop with gain, filter, and an amplitude modulator could maintain a stream of pulses separated by empty intervals (ones and zeros), in spite of the spontaneous emission noise associated with gain. In this way, a fiber ring could act as a storage ring of a bit-stream of optical pulses. This year, we demonstrated the storage principle with an experimental fiber ring containing 66 bits at a 1 GHz rate.[9]

The system consists of two rings; one serves as the pulse pattern generator, the other as the storage ring. The pulse pattern generator is simply a ring laser with a modelocking element which, starting from noise, reaches a steady state with pulses in some of the time slots and "zeros" in other slots. Figure 2 (top) shows such a bit pattern. The "zeros" turn out to be pulses as well, but of much lower peak amplitude. Through the $LiNbO_3$ switch this pattern is injected into the storage ring. Figure 2 (bottom) shows the pattern in the ring. The "zeros" have been improved so that they are now pulses of much lower amplitude than the "ones." The storage was on a time scale of hours (as long as the gain was maintained). We have addressed the stability and timing issue theoretically,[10] and MIT Lincoln Laboratory, interested in high bit-rate optical storage, has built a storage ring according to the same design and an 18 Gb/s bit-stream was stored. No physical principle prevents the upscaling of this storage to bit-rates of 100 Gb/s, if 100 GHz modulators become available.

In the upcoming year, we will determine various means for loading and unloading the storage ring. Also, we will explore the possibility of asynchronous phase modulation for storage application. If operation with an asynchronous modulation is feasible, then loading and unloading of bit-packets would be greatly facilitated.

1.3 Long-Distance Fiber Communications

Sponsors

MIT Lincoln Laboratory
National Science Foundation
Grant ECS 90-12787

---

8 H.A. Haus and A. Mecozzi, "Long-Term Storage of a Bit Stream of Solitons," *Opt. Lett.* 17: 1500-1502 (1992).

9 C.R. Doerr, W.S. Wong, H.A. Haus, and E.P. Ippen, "Additive-Pulse Mode Locking/Limiting Storage Ring," in *Conference on Lasers and Electro-Optics*, OSA Technical Digest Series, vol. 8 (Washington, D.C.: Optical Society of America, 1994), pp. CPD12-1/27 - CPD12-2/28; C.R. Doerr, W.S. Wong, H.A. Haus, and E.P. Ippen, "Additive-Pulse Mode Locking/Limiting Storage Ring," *Opt. Lett.* 19(21): 1747-1749 (1994).

10 J.D. Moores, W.S. Wong, and H.A. Haus, "Stability and Timing Maintenance in Soliton Transmission and Storage Rings," *Opt. Comm.* 113: 153-175 (1994).

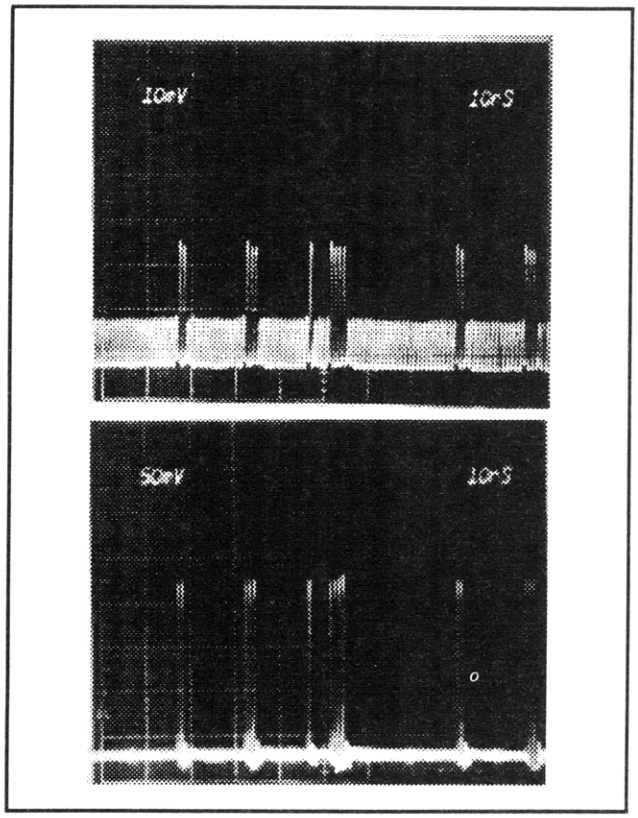

Figure 2. Example of loading. (Top) Oscilloscope trace of a bit pattern in ring number 1 (started from noise); (bottom) Oscilloscope trace of a bit pattern in ring number 2 after being loaded from ring number 1 using a 90 ns electrical gate. Horizontal scale is 10 ns/div.

Project Staff

Professor Hermann A. Haus, Farzana I. Khatri, John D. Moores, William S. Wong

We have continued to develop analytical theory and to simulate soliton propagation on the computer. In particular, we concentrated on the long-range interaction effects between solitons. When a soliton is perturbed nonadiabatically by gain, lumped filters, or loss segments, it sheds continuum. The continuum spreads away from the perturbed soliton and hits neighboring solitons. This continuum is not orthogonal to the neighboring soliton and shifts its frequency and position. These shifts are very small. However, if they are frequent enough, they can cause bit-errors.

We have developed an analytical theory for these interactions which we checked against computer simulations finding satisfactory agreement. While these effects are not large enough to cause increased bit-error rates in transoceanic transmission at the projected rates of 5 to 10 Gb/s, they could become more severe for higher bit-rates and are likely to have been observed in loop experiments conducted by Dr. Linn Mollenauer at AT&T Bell Laboratories over distances of 20,000 km or more. In his experiments, anomalous errors were attributed to piezo-optic effects produced by the solitons, but it is likely that these continuum interactions also contributed to the bit-error rate. We intend to compare our theory with past and future experiments at AT&T Bell Laboratories.

1.4 Squeezing

Sponsors

Charles S. Draper Laboratories
Contract DL-H-467138
Fujitsu Laboratories
National Science Foundation
Grant ECS 90-12787

Project Staff

Professor Hermann A. Haus, Professor Erich P. Ippen, Keren Bergman, Luc Boivin, Christopher R. Doerr, Dr. Matasaka Shirasaki

The purpose of squeezing optical radiation is to provide means for interferometeric measurements with reduced noise, at noise levels less than shot noise. We are continuing our successful experiments in squeezing. Our present aim is to improve the shot noise reduction, which is currently 5.1 dB.[11] This will be done by Luc Boivin with a system under construction which uses a high repetition rate Ti:Sapphire laser. By moving into this wavelength range, we may utilize fibers with large positive dispersion and detectors of higher quantum efficiency than for detectors at 1.3 μm wavelength. The dispersion-free fiber at 1.3 μm produced squeezing with gaussian pulses that maintained their gaussian shape throughout. In homodyne detection, the phase of the local oscillator does not align with the phase of maximum squeezing across the pulse profile. In simplest terms, a square pulse would not suffer from this drawback, realizing the full noise reduction over its entire width. Since square pulses are difficult to generate without incurring excessive power loss, we have explored theoretically the

[11] K. Bergman, H.A. Haus, E.P. Ippen, and M. Shirasaki, "Squeezing in a Fiber Interferometer with a Gigahertz Pump," *Opt. Lett.* 19: 290-292 (1994).

squeezing in a fiber with built-in pulse shaping.[12] A positively dispersive fiber, starting with a gaussian pulse, can produce better shot noise reduction than a pulse in a zero-dispersion fiber.

The high repetition rate modelocked Ti:Sapphire is of a new design pioneered by Professor James G. Fujimoto and his student Malini Ramaswamy-Paye. The repetition rate of the pulses in a squeezing experiment must be 1 GHz or higher to avoid convolution of the guided acoustic wave brillouin scattering noise into the low frequency detection window. Theoretical work on quantum noise also continues to provide new insight.[13]

1.5 Optical Channel Dropping Filters

Sponsors

National Center for Integrated Photonics
National Science Foundation
Grant ECS 90-12787

Project Staff

Professor Hermann A. Haus, Professor Leslie A. Kolodziejski, Professor Henry I. Smith, Jerry C. Chen, Jay N. Damask, Juan Ferrera, Mohammed J. Khan, Vincent V. Wong

We have begun to fabricate quarter-wave shifted distributed feedback (DFB) resonators in silica on Si using e-beam lithography. In order to produce gratings of reproducible quality, it was necessary to reduce the stitching error between e-beam fields to less than five nanometers. This has been accomplished by a new technique developed by Professor Henry I. Smith and his students, the spatial-phase-locked e-beam lithography described elsewhere in this report. The measured response of an in-line quarter wave shifted DBR resonator is shown in figure 3a, and a schematic of the resonator is shown in figure 3b. A theoretically predicted response is superimposed, and is almost indistinguishable from the measured response over the stopband of the grating. The fringes are due to a Fabry-Perot effect between the imperfectly matched waveguide input and the front of the grating. This artifact can be removed by AR coatings of the facets. On the short-wavelength side of the grating, the loss due to radiation into the substrate is clearly discernible.

The next step is to fabricate resonators side-coupled to a "signal" waveguide. For acceptable performance, the grating waveguide and the "signal" waveguide must be synchronous. Because the two waveguides are subjected to different processing steps, synchronism is not easily accomplished. Jay N. Damask has made extensive studies of the synchronism requirement and the fabrication steps required to achieve synchronism with a sufficient degree of accuracy.[14]

Other possibilities for channel dropping filter design have been explored theoretically. In collaboration with Professor John D. Joannopoulos of the Physics Department, we have started to explore the use of photonic bandgap structures for filter applications. Photonic bandgap structures have large reflections per cell, and thus a wide bandgap. With such structures, it would be possible to cover the entire bandwidth of erbium amplifiers (40 nm). Further, a single resonator becomes only a few wavelengths long. Thus, through coupling of such resonators, compact optical filters with sophisticated response characteristic could be constructed. One serious problem that must be overcome in such structures is the loss via radiation into the substrate. Computer simulations by Jerry C. Chen and some analytic modeling predict (radiation-loss) Qs as high as 20,000.[15]

Active filters (containing gain) have very interesting properties of their own. Spurious resonances can be suppressed much more effectively with active filter design than with passive ones. Further, the filters can be tuned by changes in reflection, rather than index. Since reflection is varied much more

---

[12] C.R. Doerr, M. Shirasaki, and F.I. Khatri, "Simulation of Pulsed Squeezing in Optical Fiber with Chromatic Dispersion," *J. Opt. Soc. Am. B* 11: 143-149 (1994).

[13] H.A. Haus, "From Classical to Quantum Noise," submitted to *J. Opt. Soc. Am. B* (based on Frederic Ives Medal lecture); L. Boivin, F.X. Kärtner, and H.A. Haus, "Analytical Solution to the Quantum Field Theory of Self-phase Modulation with a Finite Response Time," *Phys. Rev. Lett.* 73: 240-243 (1994); F.X. Kärtner, D.J. Dougherty, H.A. Haus, and E.P. Ippen, "Raman Noise and Soliton Squeezing," *J. Opt. Soc. Am. B* 11: 1267-1276 (1994); M. Shirasaki, I. Lyubomirsky, and H.A. Haus, "Noise Analysis of Mach-Zehnder Squeezer for Nonclassical Input State," *J. Opt. Soc. Am. B* 11: 857-863 (1994); J.K. Bounds and H.A. Haus, "Quantum Noise of Raman Amplification," *Quant. Opt.* 6: 79-85 (1994).

[14] J.N. Damask, J. Ferrara, V.V. Wong, H.I. Smith, and H.A. Haus, *Proc. SPIE* 2213: 137 (1994).

[15] J.C. Chen, H.A. Haus, J.N. Winn, and J.D. Joannopoulos, "Wide Stop Band Optical Filters from Photonic Band Gap Air Bridges," in *Guided-Wave Optoelectronics: Device Characterization, Analysis, and Design* (New York: Plenum Press), forthcoming.

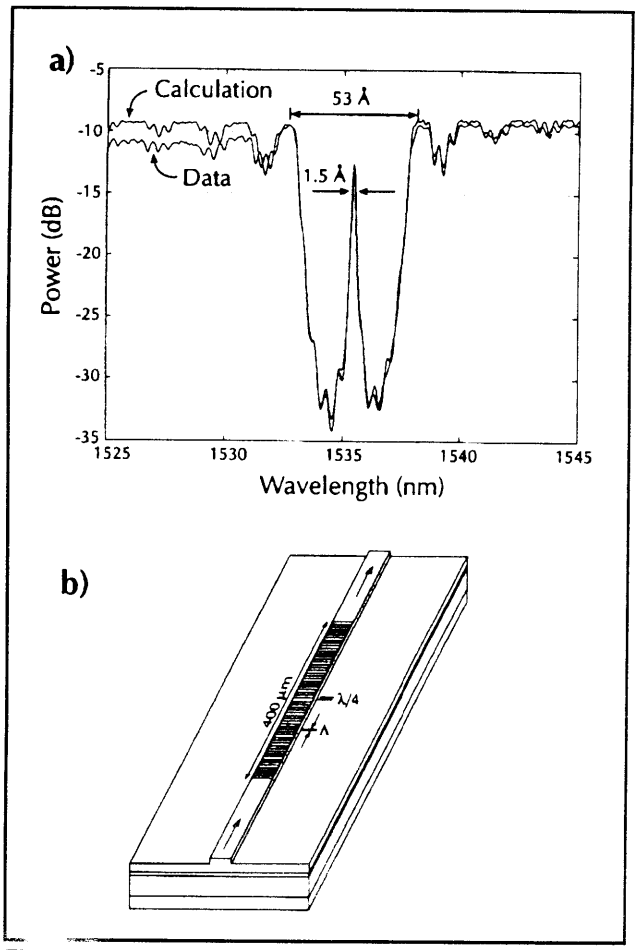

Figure 3. (a) Overlay of calculated and measured response of an in-line quarter wave shifted DBR resonator. (b) Schematic of device.

easily than the index, wider tuning ranges are possible. We have made extensive studies of such active DFB filter structures.

1.6 Overdriven Additive Pulse Modelocking

Sponsors

Joint Services Electronics Program
Contract DAAL03-92-C-0001
Grant DAAH04-95-1-0038
U.S. Air Force - Office of Scientific Research
Contract F49620-91-C-0091

Project Staff

Professor Erich P. Ippen, Professor Hermann A. Haus, Gadi Lenz, Farzana I. Khatri, John D. Moores

Overdriven additive pulse modelocking (APM) is a recent technique for passively modelocking solid state and all-fiber lasers. The principle behind APM involves splitting a pulse into two pulses which accumulate differential phase profiles. One pulse is sent through a nonlinear medium and accumulates an intensity-dependent phase profile. The pulses are then interferometrically superimposed so that they add constructively at the peak and destructively in the wings. This produces a shorter pulse. This artificial fast saturable absorber action can be achieved in a single-cavity (via a Mach-Zehnder interferometer or interference of two polarizations) or a coupled-cavity arrangement. In the NaCl:OH^- laser system, we use a coupled-cavity scheme with a gain medium in the main cavity and a nonlinear fiber in the auxiliary cavity.

Recently, we have observed "overdriven" operation of our NaCl:OH^- APM laser[16] in which the laser operates very stably, producing shortpulses with very high, nonlinear phase shifts in the auxiliary fiber. This mode of operation is difficult to analyze with our conventional APM theory which assumes small nonlinear phase shifts in the fiber. In order to understand this mode of operation, we developed a new analytical theory which looks at this overdriven case.[17] In this theory, we propose that filtering provided by bulk optical elements in the laser allows the laser to operate with these large nonlinear phase shifts. Our theory takes the usual Master Equation of APM and treats the operation of the auxiliary cavity with a new operator. Furthermore, we use Gaussian-shaped pulses as an approximate solution in order to simplify the mathematics. Using this theory along with numerical simulations, we obtain results which are in good agreement with experimental results.

Another feature of this overdriven system is a hysteretic behavior we observed which was uncharacteristic of conventional APM systems. We observed a direction-dependence of the laser operation depending on if the auxiliary cavity length was lengthened or shortened. While the cavity length is lengthened, ordinary APM behavior occurs. Pulsing

[16] G. Lenz, J. Paye, F.I. Khatri, J.D. Moores, H.A. Haus, and E.P. Ippen, "Recent Developments in Additive Pulse Modelocking of Solid State Lasers," invited paper UOE/SSL1.4, IEEE Lasers and Electro-Optics Society 1993 Annual Meeting, San Jose, California, November 1993.

[17] F.I. Khatri, G. Lenz, J.D. Moores, H.A. Haus, and E.P. Ippen, "Extension of Coupled-Cavity Additive Pulse Mode-Locked Laser Theory," *Opt. Comm.* 110: 131-136 (1994).

is intermittent, corresponding to each wavlength of detuning. However, when the cavity is shortened, pulsing begins and persists over several wavlengths. In addition, the output pulses experience a spectral red-shift as their intensity increases. We have proposed an explanation for this behavior which is based upon the saturation of the artificial fast saturable absorber action.[18] The explanation involves the nonlinear gain curve for a self-limited additive pulse modelocked laser[19] and will be described in detail in a forthcoming publication.

1.7 A Broadband-Tunable Femtosecond Source for 1.55 μm Diagnostics

Sponsors

Joint Services Electronics Program
Contract DAAL03-92-C-0001
Grant DAAH04-95-1-0038
National Center for Integrated Photonics
U.S. Air Force - Office of Scientific Research
Contract F49620-91-C-0091

Project Staff

Professor Erich P. Ippen, Gadi Lenz, Kohichi R. Tamura

Modern lightwave communication systems use carrier wavelengths around 1.55 μm because optical fibers have minimum losses and can be tailored to have negligible dispersion in this spectral region. Since all-optical systems are desirable, other communication system components need to operate around this wavelength as well. These include semiconductor laser diodes, detectors, optical amplifiers, and modulators. The characteristics of these components depend strongly on the material they are made of, the structure of the device, and the wavelength at which they are used. The probe lasers used for diagnostics need to be able to resolve ultrafast transient behavior, and be broadly tunable around 1.55 μm.

Fiber lasers have recently emerged as new sources in this spectral region. Ultrashort pulses can be obtained from these lasers by a passive modelocking technique known as stretched-pulse additive pulse modelocking (SP-APM). We have demonstrated that when pumped with a high power master oscillator power amplifier (MOPA) diode, this SP-APM laser can produce pulse energies up to 2.25 nJ in highly-chirped 1.5 ps pulses, which may then be compressed to less than 90 fs duration and more than 1.5 nJ per pulse.[20] In this mode of operation we have also found that the laser exhibits extremely low amplitude noise (less than 0.1 percent from 0 to 200 KHz), making this an excellent source for pump-probe measurements and also a seeding source for an optical amplifier.

Although these pulse energies are suitable for a variety of experiments, for many applications higher pulse energies are required. In collaboration with W. Gellerman of the University of Utah, we have built an optical amplifier for the purpose of reaching these energies.[21] We have achieved a gain of $> 10^4$ yielding ~10 μJ pulses using this system. Our amplifier uses a 2-cm-long piece of KCl:Tl^+ crystal as the gain medium, which is pumped by a Q-switched Nd:YAG at a rate of 1 KHz. To match the pump repetition rate, we have set up a synchronized electro-optic pulse selection system which selects single pulses at the 1 KHz rate from the 40 MHz output pulse train of the SP-APM fiber laser. The amplified pulse passes through the amplifier only twice resulting in excellent beam quality. The amplified pulse has been compressed to 250 fs. With further optimization, we expect to achieve even more energy per pulse and shorter pulses. These energies will allow continuum generation and make possible new time resolved spectroscopy experiments. These experiments will yield new information on the basic physics of optical devices.

---

[18] G. Lenz, J.D. Moores, F.I. Khatri, E.P. Ippen, and H.A. Haus, "Hysteresis in Highly Overdriven Additive Pulse Modelocked Laser Systems," Paper SS5.4, IEEE Lasers and Electro-Optics Society 1994 Annual Meeting, Boston, Massachusetts, November 1994.

[19] F.I. Khatri, J.D. Moores, G. Lenz, and H.A. Haus, "Models for Self-Limited Additive Pulse Mode-Locking," *Opt. Comm.* 114: 447-452 (1995).

[20] K. Tamura, C.R. Doerr, L. Nelson, H.A. Haus, and E.P. Ippen, "Technique for Obtaining High-energy Ultrashort Pulses from an Additive-pulse Mode-locked Erbium-doped Fiber Ring Laser," *Opt. Lett.* 19: 46-48 (1994).

[21] G. Lenz, W. Gellerman, E.P. Ippen, and K.R. Tamura, "Stretched-Pulse Mode-Locked Er-Doped Fiber Laser Amplified by KCl:Tl^0 Color-Center Crystals," Conference on Lasers and Electro-Optics/Quantum Electronics and Laser Science, Baltimore, Maryland, May 21-26, 1995, paper CWI3.

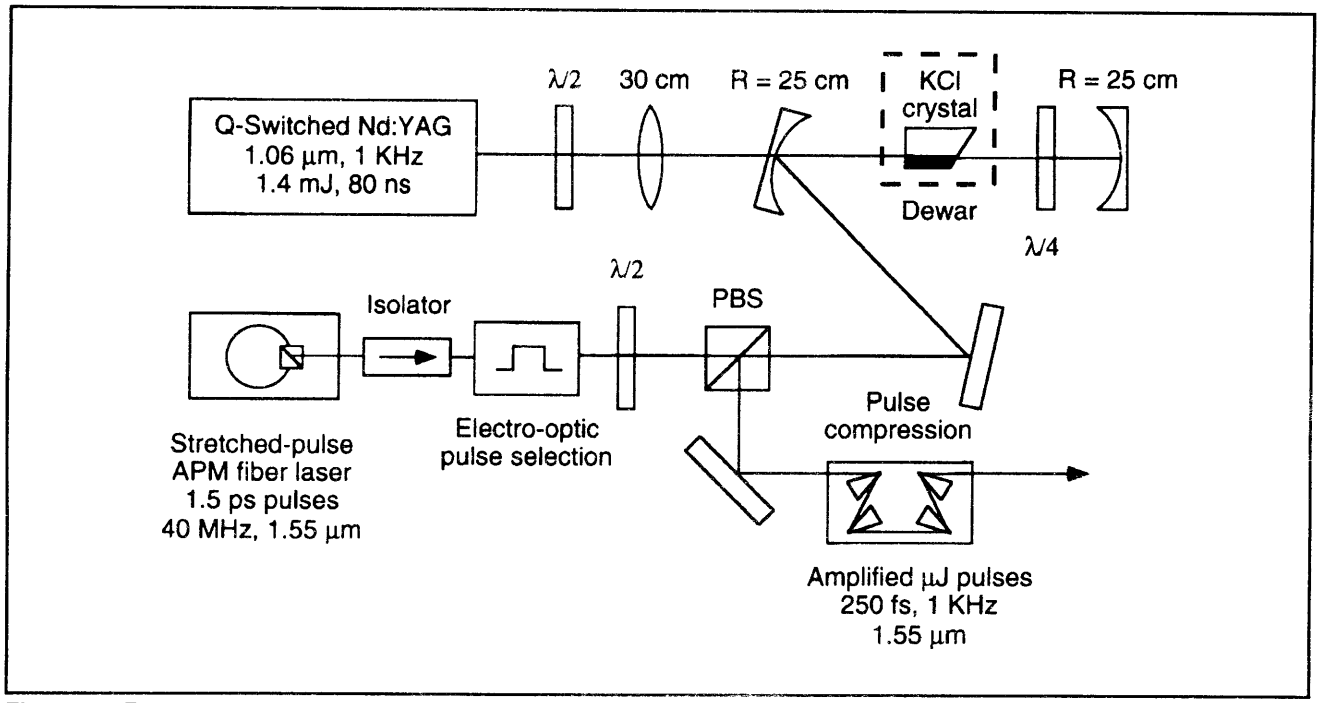

Figure 4. Experimental setup of amplified fiber laser.

1.8 Ultrafast Nonlinearities in Active Semiconductors

Sponsors

Joint Services Electronics Program
Contract DAAL03-92-C-0001
Grant DAAH04-95-1-0038
National Center for Integrated Photonics
U.S. Air Force - Office of Scientific Research
Contract F49620-91-C-0091

Project Staff

Professor Erich P. Ippen, David J. Dougherty, Charles T. Hultgren, Gadi Lenz

We have continued our investigation of nonlinear optics and ultrafast dynamics in semiconductor optical amplifiers (SOAs).[22] The active nature of these devices makes it possible to bias them electronically to produce optical gain or eliminate unwanted long-lived nonlinear components associated with carrier density dynamics. The injected carriers also introduce novel optical nonlinearities that affect ultrashort-pulse propagation in amplifiers and may potentially be used for controlling one optical pulse with another.

Measurements of gain and index of refraction dynamics have been performed by femtosecond pump-probes over a wide of photon energy in AlGaAs SOAs.[23] Our broadly-tunable femtosecond Ti:sapphire laser makes it possible to study these nonlinearities throughout the gain region and below band, as well as near the transparency point that has been investigated in detail before. Using a time-division interferometer (TDI), we have performed pump-probe of both the optically-induced transmission dynamics and the index of refraction dynamics. Below band, the transmission dynamics are dominated by the instantaneously responding two-photon absorption that is essentially independent of wavelength and bias current. The index dynamics, however, exhibit a fast, negative dynamic with a bandgap resonant component that varies by more than a factor of ten with bias current and wavelength, in agreement with recent theory.[24] There is also a slower dynamic that provides proof

---

[22] K.L. Hall, G. Lenz, A.M. Darwish, and E.P. Ippen, "Subpicosecond Gain and Index Nonlinearities in InGaAsP Diode Lasers," *Opt. Comm.* 111: 589-612 (1994).

[23] C.T. Hultgren, *Femtosecond Nonlinearities in AlGaAs Diode Laser Amplifiers*, Ph.D. diss., Dept. of Electr. Eng. and Comput. Sci., MIT, 1994.

[24] M. Sheik-Bahae and E.W. Van Stryland, "Ultrafast Nonlinearities in Semiconductor Laser Amplifiers," *Phys. Rev.* 50: 14171-8 (1994).

of nonequilibrium carrier heating. It is characterized by a 100 fs risetime related to Fermi equilibration and a 1.1 psec relaxation determined by the carrier-lattice energy exchange rate in this material. In above-band also, we have observed large variations of gain and index nonlinearity with bias current. Stimulated emission contributes to either carrier heating or cooling depending upon wavelength, and wavelength-varying gain couples ultrafast index changes to transmission dynamics. The results of all these studies can now be used to improve modeling of ultrafast device characteristics. The strength of the observed nonlinearities, and their dependence on controllable device parameters, make them interesting also for all-optical pulse control and switching applications.

In collaboration with J. Wiesenfield, M.A. Newkirk, U. Koren, and R.M. Jopson of AT&T Bell Labs, we have begun a new set of studies on SOAs fabricated to have polarization insensitive gain. This polarization insensitivity is achieved by alternating compressive and tensile strained quantum wells in the active region.

Because of polarization selection rules, the compressive wells provide gain only for light polarized in the plane of the wells (TE), while tensile wells provide gain mainly to light polarized perpendicular (TM). The resulting small signal gain is made polarization independent, but the nonlinear dynamics are not necessarily so. By using a heterodyne pump-probe scheme developed in our lab,[25] we are able to investigate these dynamics with any combination of TE or TM pump and probe pulses. Varying the relative polarization between pump and probe chances the measurement sensitivity to processes occurring in different wells. For example, when the pump is TM polarized and the probe TE, the pump will induce interband transitions primarily in the tensile wells and the probe will monitor population in the compressive wells. Thus, we may investigate inter-well transport as well as intra-well relaxation. Preliminary experiments have revealed some subpicosecond anisotropy in the dynamic gain response.[26] Future work will quantify these results and provide information about their dependence on quantum-well dimension and other device parameters.

1.9 Nonlinear Interactions of Continuous and Pulsed Light in Optical Fibers

Sponsors

Joint Services Electronics Program
Contract DAAL03-92-C-0001
Grant DAAH04-95-1-0038
U.S. Air Force - Office of Scientific Research
Contract F49620-91-C-0091

Project Staff

Professor Erich P. Ippen, David J. Dougherty

Because of their short duration, modelocked pulses have a broad spectrum. An ultrashort pulse system can be useful in nonlinear spectroscopy for this feature alone without considering its time resolving capability.

We have used the wide spectrum available from self-phase modulated 100 fs pulses from a Titanium Sapphire laser to accurately and directly measure the Raman gain spectrum of glass optical fibers. The pulses were counter-propagated through 700 meters of fiber against light from a continuous laser whose frequency lay in the middle of the pulses' spectrum. The CW laser modulated the different wavelength components of the pulse train via stimulated Raman scattering. By measuring this modulation spectrum with a spectrometer at the fiber output, we were able to extract the full Raman gain spectrum from 13 THz down to approximately 100 GHz. This approach is much simpler than measuring the gain spectrum point by point with a CW tunable probe laser.

Of course, modelocked pulses are not completely equivalent to a bright broad band incoherent source. The definite relationship between the time and frequency characteristics of the pulses permits observation of new effects which would not occur in nonlinear gain measurements of this type using inconerent light.[27] An effect of this type was discovered in our Raman gain experiment. The left hand plot in the figure shows the measured Raman gain

---

[25] K.L. Hall, G. Lenz, E.P. Ippen, and G. Raybon, "Heterodyne Pump-Probe Technique for Time-Domain Studies of Optical Nonlinearities in Waveguides," *Opt. Lett.* 17: 874-876 (1992).

[26] G. Lenz, E.P. Ippen, J.M. Wiesenfeld, M.A. Newkirk, U. Koren, and R.M. Jopson, "Anisotropy in the Ultrafast Nonlinear Response of Semiconductor Optical Amplifiers with Polarization Insensitive Gain," *Proceedings of CLEO '95, Optical Society of America,* forthcoming.

[27] D.J. Dougherty, F.X. Kärtner, H.A. Haus, and E.P. Ippen, *Opt. Lett.* 22: 276 (1994).

spectrum at small detuning for several lengths of fiber. The curve at positive Stokes detuning is the Raman gain which decreases towards zero detuning where it is masked by scattered pump light and the Brillouin gain peak at 20 GHz. At negative detuning the mirror image anti-Stokes raman spectrum is seen with an oscillatory signal superimposed.

These oscillations are a direct result of the connected time and frequency structure of the strongly chirped probe pulses. The chirp on the pulses due to the positive group velocity dispersion (GVD) of glass at 800 nm means that the red frequency components of the pulse travel ahead of the blue components. This implies that at a fixed point in the fiber, the Stokes gain of the probe occurs before the anti-Stokes gain. An excitation left in the glass by the Stokes frequencies can potentially effect the propagation of the anti-Stokes frequencies. For the highly damped Raman modes, no excitation is left behind. However, the central portion of the probe at the lowest frequencies can beat with the pump field to drive sound waves in the glass which result in Brillouin scattering of the backward traveling pump into the direction of the probe. This extra field impresses a time-dependent phase shift on the co-propagating anti-Stokes side of the probe through interference terms in the Kerr effect. The chirp causes this oscillatory phase modulation waveform in the time domain to appear directly in the spectral domain because different frequency components travel with different delays behind the center frequency. If the chirp were constant down the fiber, the spectral oscillations would extend over the entire anti-Stokes side of the probe. However, GVD stretches the duration of the probe pulse continously and most of the oscillations are washed out. Results for several fiber lengths shown in figure 5 show the modulation extending further with shorter fibers. Calculations shown in the right hand plot of the effect of this Kerr phase shift on the probe's spectrum including effects of GVD wash out agree well with experimental results.

A thermal white light source probe would not reveal this coupling mechanism in its spectrum. Although this phenomena was a nuisance for our Raman experiment, use of such a chirped probe was fortuitous for detecting the effect itself, which would appear more subtly in other situations. For instance, a train of solitons propagating against a CW background will shed these Brillouin wake fields the same as in our experiment. The consequence in this case will be merely a phase or frequency shift on the trailing pulses' spectrum rather than pronounced oscillations. This may contribute excess timing jitter in communications applications or may be judiciously used to cancel soliton self-frequency shift. In analog CW communication systems operating at power levels near the Brillouin threshold, these phase modulations could result in excess noise at channel frequencies detuned much greated than the Brillouin linewidth from the carrier. While these specific ideas are being pursued with further experiments, a more important result of this study is that small amounts of Brillouin scattering can cause observable indirect effects in certain short-pulse, broad-bandwidth applications where its direct effects can be safely neglected.

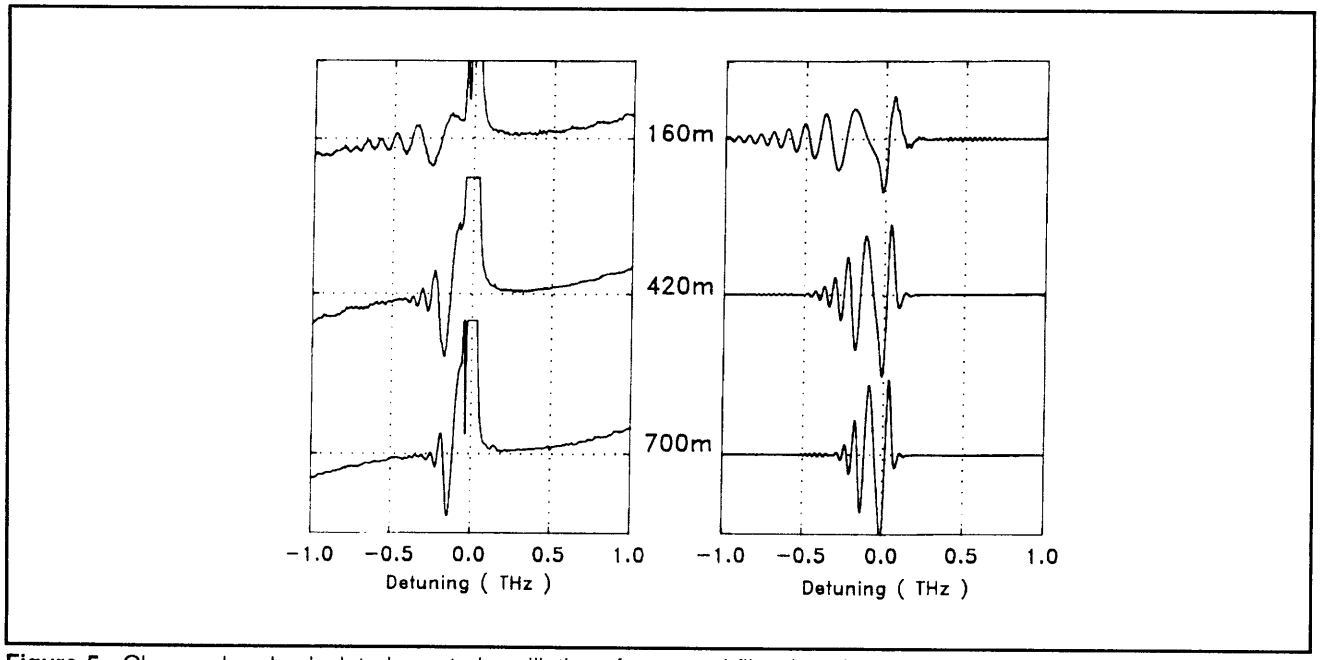

Figure 5. Observed and calculated spectral oscillations for several fiber lengths.

1.10 Intensity Autocorrelation of Light Sources for Fiber Optical Gyroscopes

Sponsors

Honeywell Technology Center
Joint Services Electronics Program
Contract DAAL03-92-C-0001
Grant DAAH04-95-1-0038

Project Staff

Professor Erich P. Ippen, David J. Dougherty, Siegfried B. Fleischer

The statistics of the light used for fiber optical gyroscopes (FOG) have a considerable effect on the rotation rate error.[28] This artifact is caused by the optical Kerr effect (n_2) of the fiber. The intensity dependent nonreciprocal phase shift has components due to self-phase modulation (SPM) and cross phase modulation (XPM) for both counter propagating beams in the Sagnac loop. The relative contributions from SPM and XPM depend on the intensity statistics of the light source. In order to cancel the Kerr effect both, the SPM and XPM have to be made equal. Then, the rotation rate error vanishes even for coupling ratios that differ from the ideal 50 percent.[29] This requires that the variance of the intensity fluctuations be $\sqrt{2}$ times the average intensity.

Theory predicts that the light emitted from a light emitting diode (LED) is Poisson, and the nonreciprocal phase shift cancels for such a source. For a practical gyroscope, one either uses a super luminecent diode or a laser diode driven below threshold. Both these devices also give, at least theoretically, vanishing rotation rate error. In practice, however, both sources are very sensitive to backreflections, which can affect the source statistics, and thus overcompensate for the rotation rate error.

To investigate intensity fluctuation properties of these sources under various conditions applicable to a commercial gyroscope, an intensity autocorrelator based on second harmonic generation was built. This autocorrelator resembles the experimental setup used to measure the pulse width of ultrafast optical pulses by means of a background-free collinear autocorrelation. The light emitted from the diode is split into two parts and, after propagating through two distinct paths with adjustable difference, focused into an SHG crystal. The measured SHG intensity is proportional to the second-order coherence function of the light.

To preserve the light statistics, care was taken to balance the dispersion between both beams and to ensure upconversion of the whole spectrum. Because of the large bandwidth of the source a, very thin and broadband doubling crystal was selected (100 μm BBO). This results in a very low (10^{-9}) SHG conversion efficiency for the incoherent, low-power sources, and a photon counting detection system was needed.

The measured second-order coherence functions agree with what is predicted for a chaotic source with the given spectrum (first order coherence function). The contrast ratios of the intensity autocorrelations; however, differ in various ways from those expected. We believe that these deviations are mostly is due to artifacts of the different measurement geometries. A contrast ratio $G^{(2)}(0)/G^{(2)}(\infty) = 1.93$ was obtained using type II phasematching in the BBO crystal. This is close enough to the value 2.0 expected from Poisson statistics to provide confidence that the light of these sources can be chaotic. Reduction of backscatter turned out to be very critical. How residual backreflections into the diode affect the measured statistics of the light is currently being investigated.

1.11 Wavelength Shifting by Four-Wave Mixing in Passive Semiconductor Waveguides

Sponsors

Joint Services Electronics Program
Contract DAAL03-92-C-0001
Grant DAAH04-95-1-0038
National Center for Integrated Photonics
U.S. Air Force - Office of Scientific Research
Contract F49620-91-C-0091

Project Staff

Professor Erich P. Ippen, Ali M. Darwish, Gadi Lenz

---

[28] S. Ezekiel, J.L. Davis, and R.W. Hellwarth, "Non-Reciprocal Errors Sources," *Fiber-Optic Rotation Sensors and Related Technologies* 332 (1982).

[29] R.A. Bergh, B. Culshaw, C.C. Cutler, H.C. Lefere, and H.J. Shaw, "Source Statistics and the Kerr Effect in Fiber-Optic Gyroscopes," *Opt. Lett.* 7: 563 (1982).

To investigate devices for wavelength-division-multiplexed (WDM) optical network applications, we are performing all-optical, wavelength-shifting experiments in semiconductor waveguides at 1.55 μm, in collaboration with H.Q. Le, J.P. Donnelly, S.H. Groves and Eric A. Swanson of Lincoln Laboratory. The wavelength-shifting is accomplished by non-degenerate four-wave mixing (FWM) which uses optical beams at two different input wavelengths (signal-in and pump) to generate output at a third wavelength (signal-out). Since the mixing process depends upon instantaneous field products, there is no response-time limit in the time domain. Instead, the nonlinearity response time of the medium manifests itself as variation of conversion efficiency with magnitude of the wavelength shift. To investigate the possibility of obtaining a relatively flat conversion efficiency over a wide detuning range, we are studying InGaAsP/InP passive waveguides. We have performed both cw experiments and picosecond pulse experiments at 1.55 μm wavelengths, with tunable, synchronized F-center lasers, to evaluate: variations of efficiency with pump wavelength (below band), the effects of phase matching on shifts as large as 130 nm (17 THz), and the limitations on conversion imposed by two-photon absorption. Our data allows us to extract quantitative values for waveguide loss, group-velocity dispersion, and both the real and imaginary parts of $\chi^{(3)}$. Two-photon absorption, strictly a liability in nonlinear index switching, can actually enhance FWM conversion efficiency to some extent. We have analyzed this theoretically and quantified it experimentally.[30] In a 7.5-mm-long passive InGaAsP single quantum well waveguide, we have achieved a conversion efficiency for picosecond pulses of -11 dB for a wavelength shift of 20 nm. In a waveguide with an effective mode area of 3×10^{-3} cm^2, this requires a pump pulse energy of 10 nJ in 10 ps. The waveguide structures are fabricated at Lincoln Laboratory. Future plans call for optimizing design of the waveguide shifters using multiple quantum wells and incorporating a p-n junction for carrier sweep-out.

1.12 Ultrashort Pulse Generation in Solid State Lasers

Sponsors

Joint Services Electronics Program
Contract DAAL03-92-C-0001
Grant DAAH-04-95-1-0038
U.S. Air Force - Office of Scientific Research
Contract F49620-91-C-0091
U.S. Navy - Office of Naval Research (MFEL)
Contract N00014-94-1-0717

Project Staff

Dr. Brett E. Bouma, Malini Ramaswamy-Paye, Dr. Joseph A. Izatt, Professor James G. Fujimoto, Dr. Jeffrey Russell,[31] Dr. Raymond Sierra,[31] Professor Ursula Keller[32]

1.12.1 Compact Ultrashort Pulse Sources

Compact ultrashort pulse sources are of fundamental importance for advances in signal processing, high speed communications, and the investigation of ultrafast nonlinear processes in semiconductor devices and materials. Generally, these sources must be technologically simple, robust and cost effective. While solid state gain media are well suited to meet these criteria, their relatively low gain cross-sections have required the use of fast saturable absorption for modelocking. During the last few years significant advances have been made in the development of fast saturable absorbers utilizing the electronic Kerr effect. Kerr lens modelocking (KLM),[33] in fact, has allowed the generation of the shortest pulses ever produced directly from a laser oscillator.[34] A theoretical understanding of Kerr effect modelocking has been

---

[30] A.M. Darwish, G. Lenz, E.P. Ippen, H.Q. Le, J.P. Donnelly, S.H. Groves, and E.A. Swansen, "Frequency Conversion in Passive InGaAsP/InP Waveguides," *OSA Technical Digest*, QELS '95, Optical Society of America, paper QThJ2, 1995.

[31] Candela Laser Corporation, Wayland, Massauchusetts.

[32] Swiss Federal Institute of Technology, Zürich, Switzerland.

[33] D.K. Negus, L. Spinelli, N. Goldblatt, and G. Feuget, "Sub-100 fs Pulse Generation by Kerr Lens Modelocking in Ti:Al_2O_3," *Technical Digest of the Topical Meeting on Advanced Solid State Lasers* (Washington, D.C.: Optical Society of America, 1991), postdeadline paper.

[34] J. Zhou, G. Taft, C-P. Huang, M.M. Murnane, H.C. Kapteyn, and I.P. Christov, "Pulse Evolution in a Broad-Band Ti:sapphire laser," *Opt. Lett.* 19: 1149 (1994).

developed by Professors Eric P. Ippen and Hermann A. Haus in conjunction with our group.[35]

In the past year, we have applied our theoretical model of KLM to facilitate optimization of modelocking performance and to allow the extension of this simple pulse forming mechanism to novel resonator geometries. Two Ti:Al_2O_3 KLM lasers in our laboratory, currently producing pulses of ~10 fs duration, are direct results of the accuracy of our modeling.

Chirp-free ultrashort pulses are produced in KLM as a result of a self-focusing nonlinearity in the presence of soliton-like pulse shaping arising from self-phase modulation and net negative intracavity group-velocity dispersion (GVD). Negative GVD is most commonly achieved in KLM lasers by use of an intracavity prism pair; however, this places constraints on laser geometry and size. To date, KLM lasers have almost exclusively used a folded X- or Z-cavity geometry with the prism pair in one arm of the laser. Repetition rates have not exceeded the 100 MHz range.

This past year, we have developed a novel and compact dispersion-compensation technique and laser geometry for KLM in solid-state lasers.[36] This design provides built-in and easily adjustable GVD as a direct consequence of the resonator geometry, eliminating the need for prism pairs. We have produced 111 fs pulse durations at a repetition rate of 1 GHz and 54 fs pulses at 385 MHz. The demonstrated geometry has important implications for compact, all-solid-state, femtosecond laser technology, especially because it can readily be extended to the modelocking of diode-pumped lasers.

1.12.2 Cavity Dumped Ultrashort Pulse Lasers

Femtosecond laser systems have been widely applied for the study of ultrafast phenomena in physics, chemistry, and biology. An optimum laser source for these studies should have a short pulse duration, wavelength tunability, sufficient pulse energy to permit the investigation of nonlinear effects and sufficient repetition rate to permit the use of averaging techniques for high sensitivity detection. Finally, the laser system should be simple, cost effective, and robust.

The advent of the femtosecond Kerr lens modelocked (KLM) Ti:Al_2O_3 laser was an important advance in ultrafast optics. The peak power at the output of modelocked Ti:Al_2O_3 laser sources can be in the range of 0.2 MW, significantly higher than that of modelocked dye lasers. However, for studies of nonlinear phenomena, higher peak powers are often necessary. Several amplification techniques have recently been developed to extend the range of available pulse energies from Ti:Al_2O_3 sources. Regenerative as well as multipass amplifiers with Nd:YAG and Nd:YLF pump lasers have been demonstrated up to a few kilohertz repetition rates.[37] More recently, argon laser pumped Ti:Al_2O_3 amplifiers have produced microjoule energies at repetition rates as high as 450 kHz.[38] However, the requirement of multiple stages and/or multiple pump lasers makes these oscillator plus amplifier systems complex and relatively expensive. Lastly, the repetition rate of many of these sources is low enough to limit detection sensitivity for ultrafast measurements.

A superior alternative to these laser systems, demonstrated by our group, is cavity dumping of a KLM Ti:Al_2O_3 oscillator.[39] This technique allows the generation of 50 fs pulses with pulse energies as high as 100 nJ at variable repetition rates as high as 0.95 MHz. The limitation on the energy currently available from this source arises because of mul-

---

[35] H.A. Haus, J.G. Fujimoto, and E.P. Ippen, "Structures for Additive Pulse Modelocking," *J. Opt. Soc. Am. B* 8: 2068 (1991); H.A. Haus, J.G. Fujimoto, and E.P. Ippen, "Analytic Theory of Additive Pulse and Kerr Lens Mode Locking," *IEEE J. Quant. Electron.* 28: 2086 (1992).

[36] M. Ramaswamy-Paye and J.G. Fujimoto, "Compact Dispersion-Compensating Geometry for Kerr-Lens Mode-Locked Femtosecond Lasers," *Opt. Lett.* 19: 1756 (1994).

[37] K. Wynne, G.D. Reid, and R.M. Hochstrasser, "Regenerative Amplification of 30 fs Pulses in Ti:Sapphire at 5 kHz," *Opt. Lett.* 19: 895 (1994).

[38] T.B. Norris, "Femtosecond Pulse Amplification at 250 kHz with a Ti:Sapphire Regenerative Amplifier and Application to Continuum Generation," *Opt. Lett.* 17: 1009 (1992).

[39] M. Ramaswamy, M. Ulman, J. Paye, and J.G. Fujimoto, "Cavity-Dumped Femtosecond Kerr-Lens Mode-Locked Ti:Al_2O_3 Laser," *Opt. Lett.* 18: 1822 (1993).

tiple pulse instabilities that occur at high pulse energies as a result of saturation of the KLM saturable absorber action. Decreasing the output coupling of this laser increases the cavity Q but does not enhance the dumped energies since it reduces the pump level at which multiple pulse instabilities occur. We are currently testing techniques such as defocusing the beam within the gain crystal and implementing other dumping mechanisms that do not require a focused beam so that the KLM nonlinearity can be decreased and the instability threshold, thereby, increased.

1.12.3 Flashlamp Pumped Modelocked Ti:Al_2O_3 Laser

Nearly all modelocked Ti:Al_2O_3 lasers to date have been cw modelocked systems with relatively low pulse energies. Short pulse energies in the range of microjoules to millijoules can be generated using regenerative and multipass amplifier systems. While these techniques achieve excellent performance, they are relatively costly and complex. Simple affordable sources of wavelength tunable, picosecond, high power laser pulses are relevant to applications such as frequency doubling, optical parametric oscillators, materials processing, laser surgery, and picosecond ultrafast nonlinear spectroscopy.

This past year, we have demonstrated a high performance, all solid-state, modelocked flashlamp pumped Ti:Al_2O_3 laser by combining active acousto-optic modulation and fast saturable absorber action from a low temperature multiple quantum well.[40] This laser has produced pulses as short as 4.5 ps with peak powers exceeding 4 MW at a repetition rate of 10 Hz. The flashlamp pumped Ti:Al_2O_3 laser is a simple, economical, high peak power laser source which can be an attractive alternative technology to conventional oscillator-amplifier approaches. In addition, the development of new techniques for modelocking flashlamp pumped lasers can be generalized to a broad class of new solid state laser materials currently being developed.

1.13 Ultrafast Phenomena in Materials and Devices

Sponsors

Joint Services Electronics Program
Contract DAAL03-92-C-0001
Grant DAAH-04-95-1-0038
U.S. Air Force - Office of Scientific Research
Contract F49620-91-C-0091
U.S. Navy - Office of Naval Research (MFEL)
Grant N00014-91-J-1956

Project Staff

Igor P. Bilinsky, Boris Golubovic, Morrison Ulman, Malini Ramaswamy-Paye, Chi-Kuang Sun, Dr. Brett E. Bouma, Professor Erich P. Ippen, Professor James G. Fujimoto, Professor Christopher Stanton[41]

1.13.1 Carrier Dynamics in InGaAs Strained Layer Diodes

Nonlinear gain and transient carrier dynamics in diode lasers play important roles in laser line width, modulation bandwidth, amplification, and short pulse generation. Femtosecond, multiple wavelength pump-probe measurements of nonlinear gain dynamics were performed in InGaAs/InGaAsP strained-layer multiple-quantum-well (MQW) amplifiers.[42] These studies have shown that non-equilibrium carrier temperature effects play a dominant role in nonlinear gain dynamics. Previous studies[43] have shown that free carrier absorption dominates carrier heating process. A number of experimental techniques were used to study carrier dynamics in waveguide devices such as bias lead

---

[40] B. Bouma, A. Gouveia-Neto, J.A. Izatt, J. Russell, R. Sierra, U. Keller, and J.G. Fujimoto, "Hybrid Mode Locking of a Flash-Lamp-Pumped Ti:Al_2O_3 Laser," *Opt. Lett.* 19: 1858 (1994).

[41] University of Florida, Gainsville, Forida.

[42] M.S. Stix, M.P. Kesler, and E.P. Ippen, "Observations of Subpicosecond Dynamics in GaAlAS Laser Diodes," *Appl. Phys. Lett.* 48: 1722 (1986).

[43] C.T. Hultgren, D.J. Dougherty, and E.P. Ippen, "Above- and Below-Band Femtosecond Nonlinearities in Active AlGaAs Waveguides," *Appl. Phys. Lett.* 61: 2767 (1992).

monitoring,[44] time domain interferometry,[45] and heterodyne detection.[46] These techniques, however, are based on conventional, single-wavelength pump-probe geometry. To our knowledge, preceding this work, no multiple wavelength gain and transient carrier dynamics measurements were reported.

The measurements were performed using a new heterodyne multiple wavelength pump-probe technique. A modelocked Ti:Al_2O_3 laser output spectrum was coupled into an optical fiber for self-phase modulation spectral broadening. The light coming out of the fiber was split into the pump and probe beams. Two separate spectral windowing assemblies allowed for independent frequency, pulsewidth, and polarization selection of both pump and probe pulses. Since this technique utilizes a collinear geometry, it is of particular interest for studies of guided wave optical devices. Moreover, this technique can be applied to both measurements of gain and index dynamics. The demonstrated technique represents a powerful tool for investigating device dynamics since it allows for performing temporal as well as spectral studies in a single experimental set-up.[47]

The devices investigated were InGaAs/AlGaAs graded-index separate confinement heterostructure SQW ridge waveguide diode lasers. The devices used were fabricated in collaboration with investigators at the MIT Lincoln Laboratory. The epitaxial growth of nonlattice-matched materials, strained layer quantum well devices provide an added degree of freedom to band structure engineering and optic and optoelectronic device research. High power, high efficiency, long lifetime, and low threshold current density semiconductor lasers have been achieved in the laboratory by InGaAs strained layer devices in the past few years.

Studies of the femtosecond gain dynamics were performed using the multiple-wavelength pump-probe technique. We were able to map the femtosecond gain dynamics at a range of wavelengths for a fixed excitation pulse. The transient measurements showed a pump-induced transmission decrease in both the gain and loss regions. Around zero time delay, a sharp transmission decrease was observed with a spectral peak around the pump wavelength and a time-resolution-limited recovery. This transient may be attributed to a combination of two-photon absorption, spectral hole burning, and coherent artifacts. Shortly after the pump pulse, a thermalized carrier distribution with higher temperature and lower concentration is established. Gain depletion throughout the investigated spectral region was observed. For time delays longer than 1 ps, the gain partially recovers as the temperature reaches equilibrium with the lattice. The residual gain changes are produced by the decrease in the carrier population and recover on a much longer time scale.

Under conditions of high carrier concentrations, with the pump wavelength close to the bottom of the gain region, strong spectral hole burning effects were observed. Moreover, an additional blue shift of the spectral hole with respect to the pump wavelength was observed.[48] At lower carrier concentrations with the pump close to the transparency point, spectral hole burning effects were much weaker without any spectral shifts. This new information is important to understanding gain dynamics and its implication on high speed optical device performance such as cross-talk effects, short pulse amplification, and high speed modulation behavior.

In collaboration with theoretical physicists at the University of Florida, Gainsville, a detailed theoretical model for the gain dynamics for the measured device is being developed. This aids in the full understanding of the obtained experimental results and may aid future device design. The theoretical

---

[44] K.L. Hall, E.P. Ippen, and G. Eisenstein, "Bias-Leading Monitoring of Ultrafast Nonlinearities in InGaAsP Diode Laser Amplifiers," *Appl. Phys. Lett.* 57: 129 (1990).

[45] M.J. LaGasse, K.K. Anderson, C.A. Wang, H.A. Haus, and J.G. Fujimoto, "Femtosecond All-Optical Switching in AlGaAs Waveguides using a Time Division Interferometer," *Appl. Phys. Lett.* 54: 2068 (1989).

[46] K.L. Hall, G. Lenz, E.P. Ippen, U. Koren, and G. Raybon, "Carrier Heating and Spectral Hole Burning in Strained-Layer Quantum Well Laser Amplifiers at 1.5 μm," *Appl. Phys. Lett.* 61: 2512 (1992).

[47] C.-K. Sun, B. Golubovic, J.G. Fujimioto, H.K. Choi, and C.A. Wang, "Heterodyne Nondegenerate Pump-Probe Measurement Technique for Guided Wave Devices," *Opt. Lett.* 20: 210-212 (1995).

[48] C.-K. Sun, B. Golubovic, H.K. Choi, C.A. Wang, and J.G. Fujimoto, "Femtosecond Investigations of Spectral Hole Burning in Semiconductor Lasers," *App. Phys. Lett.*, forthcoming.

work is an extension of previous collaborations,[49] and preliminary results show close agreement with experimental data obtained.

1.13.2 Nonequlibrium Electron Dynamics in Metals

Studies of interactions between free carriers and their environment constitute one of the major problems of solid state physics. This has been addressed directly in the time domain employing femtosecond techniques, both in semiconductor and metals. Of particular interest in the case of metals is the display of very high electron density whose behavior can be modeled on a relatively simple basis. In previous experiments,[50] it was demonstrated that it is possible to create and probe transient nonequilibrium electron populations using ultrashort laser pulses. In these experiments, it was assumed that electron-electron interactions were sufficiently fast to thermalize the electron gas on the order of, or shorter, than the pulse pump duration. This assumption was made even though some deviations from the instantaneous response were observed.[51] More recent investigations using transient photoemission have demonstrated the existence of non-Fermi electron distribution with thermalization times as long as 600 fs.[52] These results were observed in gold foil for large changes of the electron temperature (of the order of 400° K) with a limited time resolution. Similar conclusions were drawn at lower laser fluence by analyzing the temperature dependence of the optically measured electron-photon interaction time in gold and silver.[53]

Femtoscond studies of electron thermalization in metals were conducted using transient thermomodulation transmissivity and reflectivity. Studies were performed using a tunable multiple-wavelength femtosecond pump-probe technique in optically thin gold films in the low perturbation limit. An infra-red (IR) pump beam was used to heat the electron distribution and changes in electron distribution and electron temperature were measured with a visible probe beam at the *d* band to Fermi-surface transition.[54] These studies show that the subpicosecond optical response of gold is dominated by delayed thermalization of the electron gas. This effect is particularly important far off the spectral peak of the reflectivity or transmissivity changes, thus permitting a direct and sensitive access to the internal thermalization of the electron gas.

Measurements using a high stability, high repetition rate, and tunable, modelocked Ti:Al_2O_3 laser, show evidence for non-Fermi electron distribution. This distribution was measured to have an electron thermalization time of the order of 500 fs and an electron-lattice cooling time of 1 ps, independent of laser fluence in the range of 2.5 mJ/cm^2. At energies close to the Fermi surface, longer thermalization timer ~1-2 ps were observed. These results are in agreement with a more sophisticated model based on calculations of the electron-thermalization dynamics by numerical solutions of the Boltzman equations.[55] This model quantitatively describes the measured transient optical response during the full thermalization time of the electron gas to be of the order of 1.5 ps. Finally, the theoretical and experimental techniques developed in this study can form the basis for investigating and understanding nonthermal electronic effects in a wide range of materials.

---

[49] G.D. Sanders, C.-K. Sun, J.G. Fujimoto, H.K. Choi, C.A. Wang, and C.J. Stanton, "Carrier Gain Dynamics in InGaAs/AlGaAs Strained-Layer Single-Quantum-Well Diode Lasers: Comparison of Theory and Experiment," submitted to *Phys. Rev. B.*

[50] G.L. Eesley, "Observation of Nonequilibrium Electron Heating in Copper," *Phys. Rev. Lett.* 51: 2140 (1983).

[51] H.E. Elsayed-Ali, T.B. Norris, M.A. Pessot, and G.A. Mourou, "Time-Resolved Observation of Electron-Phonon Relaxation in Copper," *Phys. Rev. Lett.* 58: 1212 (1987).

[52] R.W. Schoenlein, W.Z. Lin, J.G. Fujimoto, and G.L. Eesley, "Femtosecond Studies of Nonequilibrium Electronic Process in Metals," *Phys. Rev. Lett.* 58: 1680 (1987).

[53] W.S. Fann, R. Storz, H.W.K. Tom, and J. Bokor, "Direct Measurement of Nonequilibrium Electron Energy Distributions in Subpicosecond Laser-Heated Gold Films," *Phys. Rev. Lett.* 68: 2834 (1992).

[54] C.-K. Sun, F. Vallée, L.H. Acioli, E.P. Ippen, and J.G. Fujimoto, "Femtosecond-Tunable Measurement of Electron Thermalization in Gold," *Phys. Rev. B* 50: 337 (1994).

[55] C.-K. Sun, F. Vallée, L. Acioli, E.P. Ippen, J.G. Fujimoto, "Femtosecond Investigation of Electron Thermalization in Gold," *Phys. Rev. B* 48: 12365 (1993).

1.13.3 Time Gated Scanning Tunneling Microscopy

Since the invention of the scanning tunneling microscope (STM) in 1982, scanning tunneling microscopy has become a well established technique that allows us to study sufaces with very high spatial resolution down to atomic dimensions. However, the temporal resolution of a conventional STM is limited to microseconds. Today, femtosecond laser technology enables measurement of the highest time resolution possible of solid state phenomena. However, the spatial resolution is limited to microns by a laser spot size. A combination of STM with ultrafast time resolution of femtosecond lasers would enable us to develop an instrument capable of performing surface measurements highly localized in both spatial and temporal domain. Recently, a number of approaches to this problem have been taken.[56]

In an STM, a sharp metal tip is positioned a few angstroms away from the surface under investigation. An electrical bias is applied between the tip and the surface. When the tip is close to the surface, a small tunneling current will flow from the tip to the surface. The size of this current depends exponentially on the distance between the tip and the sample. If we heat an electron distribution with a laser pulse, we would expect the tunneling of heated carriers to be different from that of a cold equilibrium distribution.

In our experiment, a Pt-Ir tip is positioned above an Au surface. Amplified femtosecond laser pulses are applied to the tip-sample junction of an STM and the effect of the laser pulses on the tunneling current is monitored. Several effects contribute to the laser induced tunneling current. They include three-photon photoionization and carrier heating, which in turn leads to thermally assisted photoionization and thermally assisted tunneling.[57] Time resolution is achieved by splitting a laser pulse into two pulses of equal energy and varying time delay between them. As a result, a femtosecond interferometric cross correlation is obtained. We have investigated the dependence of different components of the laser assisted tunneling current on a number of parameters including laser intensity and polarization and the STM tip-sample bias voltage.

1.14 Laser Medicine

Sponsors

National Institutes of Health
Grant NIH-5-R01-GM35459-09
U.S. Air Force - Office of Scientific Research
Grant F49620-93-1-0301
U.S. Navy - Office of Naval Research (MFEL)
Contract N00014-94-1-0717

Project Staff

Stephen A. Boppart, Michael R. Hee, Dr. Charles P. Lin, Guillermo J. Tearney, Dr. Brett E. Bouma, Dr. Joseph A. Izatt, Professor James G. Fujimoto, Eric A. Swanson,[58] Dr. Mark E. Brezinski, Dr. Reginald Birngruber,[59] Dr. Cynthia A. Toth,[60] Dr. Clarance P. Cain, Gary D. Noojin,[61] Dr. W.P. Roach, Dr. Cheryl D. DiCarlo[62]

1.15 Optical Coherence Tomography Technology

Optical coherence tomography (OCT) is a new technique that uses low coherence interferometry to gate out multiply scattered photons, and in the single scattering limit, is equivalent to time-of-flight

---

56 D.M. Bloom, A.S. Hou, and F. Ho, "Brave New Nanoworld: Probing the Realm of Ultrafast, Ultrasmall Electronics," *Ultrafast Phenomena,* Vol. 7, 1994 OSA Technical Digest Series (Washington, D.C.: Optical Society of America, 1994), pp. 298-300; S. Weiss, D. Botkin, D.F. Ogletree, M. Salmeron, and D.S. Chemla, "Advances in Ultrafast Scanning Probe Microscopy," *Ultrafast Phenomena,* Vol. 7, OSA Technical Digest Series (Washington, D.C.: Optical Society of America, 1994), pp. 301-303.

57 G. Gerber, F. Sattler, S. Vogler, J.Y. Grand, P. Leiderer, R. Möller, "Femtosecond Time-Resolution in Scanning Tunneling Microscopy," *Ultrafast Phenomena,* Vol. 7, 1994 OSA Technical Digest Series (Washington, D.C.: Optical Society of America, 1994), p. 254.

58 MIT Lincoln Laboratory, Lexington, Massachusetts.

59 Medizinisches Laserzentrum, Lubeck, Germany.

60 Duke University Eye Center, Durham, North Carolina.

61 TASC, San Antonio, Texas.

62 Armstrong Laboratory, Brooks Air Force Base, Texas.

imaging.[63] OCT is analogous to ultrasound B mode imaging except that it uses an infrared light source and low coherence interferometry to perform micron resolution ranging and imaging. For an interferometric signal to be detected, the optical pathlengths of the object and reference beam must be matched to within the coherence length of the source. Since multiply scattered photons from the object have travelled different optical pathlengths than the reference beam, multiple scattering effects are minimized in the OCT image.

An OCT system that accommodates multiple sources has been constructed. The source is coupled into a single mode fiber optic Michelson interferometer. The OCT system obtains tissue axial reflectance by varying the reference arm length and digitizing the magnitude of the demodulated interference envelope. A cross-sectional image is produced by recording axial reflectance profiles while the object beam or the tissue specimen is scanned laterally. After acquisition, the reflectance images can be displayed using false color or gray scale lookup tables chosen to enhance visualization of tissue microstructure.

The axial resolution of OCT images is determined by the coherence length of the source. When using a superluminescent diode (SLD) as the optical input, an axial resolution of less than 20 μm is achieved. This resolution is 10 times greater than the resolution obtained using conventional ultrasound, MRI, or CT. In addition, an axial resolution of 4 μm has recently been demonstrated using a modelocked Kerr lens Ti:Al_2O_3 source. Another advantage of OCT over other imaging modalities is its high detection sensitivity. Because OCT uses heterodyne detection in conjunction with other noise reduction techniques, a sensitivity of 110 dB is possible for detection of reflectance within the tissue.

This work is an ongoing collaboration with researchers at MIT, the Optical Communications Group at MIT Lincoln Laboratories, New England Eye Center of the Tufts University School of Medicine, Massachusetts General Hospital Cardiology Department, Pathology Department, and the Wellman Laboratories of Photomedicine. Lincoln Laboratories has provided much of the OCT technology and equipment for use in ophthalmic and multiply scattering tissue studies. The New England Eye Center is currently performing clinical trials using an OCT system adapted to a slit lamp for anterior and posterior diagnosis of a wide array of ophthalmic diseases. Massachusetts General Hospital has been instrumental in providing the tissue samples and pathology for research aimed at evaluating the potential for OCT to perform micron level "optical biopsies" in multiply scattering human tissue.

1.15.1 Optical Coherence Tomography for Ophthalmic Diagnosis

In collaboration with investigators at the New England Eye Center of the Tufts University Medical School, we have been investigating OCT as a new ophthalmic imaging instrument in the anterior and posterior eye. In comparison to existing ophthalmic imaging techniques such as ultrasound and scanning laser ophthalmoscopy, OCT is non-contact and has higher (10 μm) longitudinal resolution. A high-sensitivity fiber-optic OCT instrument has been constructed and is interfaced to a standard slit-lamp biomicroscope for clinical use.[64] The probe beam is coincident with the observation path of the slit-lamp permitting visualization of the scanning pattern on the anterior chamber or fundus simultaneously with biomicroscopic observation. Computer control and data acquisition allow fine positioning and orientation of the scan in the eye and digitization of the tomographic images. A real-time display of the scan in progress is available on a computer monitor, which is updated every 2.5 s. Computer algorithms have been developed for image analysis and restoration.

In the anterior eye, OCT is potentially useful for the highly accurate biometry of large scale ocular structures, and the evaluation of pathologies of the cornea, iris, and lens.[63] Preliminary tomograms have been obtained in patients with band keratopathy, keratitis, corneal edema, iridocorneal adhesions, and cataracts. The non-contact, high-resolution cross-sectional view provided by OCT is also promising for the intraoperative and post-operative evaluation of keratorefractive surgeries. As an example, we have used OCT to quantitate

---

[63] J.A. Izatt, M.R. Hee, E.A. Swanson, D. Huang, C.P. Lin, J.S. Schuman, C.A. Puliafito, and J.G. Fujimoto, "Micron-Scale Resolution Imaging of the Anterior Eye in Vivo with Optical Coherence Tomography," *Arch. Ophthalmol.* 112: 1584 (1994).

[64] J.A. Izatt, M.R. Hee, E.A. Swanson, D. Huang, C.P. Lin, J.S. Schuman, C.A. Puliafito, and J.G. Fujimoto, "Micron-Scale Resolution Imaging of the Anterior Eye *in vivo* with Optical Coherence Tomography," *Arch. Ophthalmol.* 112: 1584 (1994); M.R. Hee, J.A. Izatt, E.A. Swanson, D. Huang, J.S. Schuman, C.P. Lin, C.A. Puliafito, and J.G. Fujimoto, "Optical Coherence Tomography of the Human Retina," *Arch. Ophthalmol.*, forthcoming.

the changes in corneal edema and curvature following laser thermokeratoplasty (LTK) surgery in a rabbit model. Dynamic information on the cellular healing process is also available from sequential OCT images of a single lesion obtained over a period of several weeks. These tomograms clearly document the extent of the lesion, changes in lesion morphology with time, and provide a non-invasive, *in vivo* alternative to histopathology.

Micron-scale axial resolution is particularly important for the early diagnosis and monitoring of degenerative retinal diseases. We have examined over 600 patients at the New England Eye Center with a variety of diseases of the macula[65] and optic nerve,[66] including macular hole, retinal detachment, macular edema, age-related macular degeneration, and glaucoma. OCT images have been correlated with conventional clinical examination, fluorescein angiography, and visual field testing.

The diagnosis of macular holes, a common cause of progessive central vision loss, can be difficult. Lesions that ophthalmoscopically resemble various stages of macular hole development include lamellar holes, macular cysts, foveal detachments of the neurosensory retina or pigment epithelium, and epiretinal membranes and macular pseudoholes. OCT can effectively distinguish these pathologies in cross-section.[67] OCT can also stage idiopathic macular holes which may be important in evaluating surgical intervention. Vitreomacular traction has been implicated in the pathogenesis of hole formation. The high resolution of OCT is helpful in assessing the vitreoretinal interface which is useful for evaluating the risk of hole formation, especially in the fellow eyes of patients with a unilateral macular hole. Quantitative information may be directly extracted from the OCT tomograms, including the diameter of the hole, and the extent of surrounding subretinal fluid accumulation. The high-resolution obtained in the tomographs suggests that OCT may be a useful method of precisely monitoring hole progression, or recovery after surgery.

Macular edema is commonly associated with diabetic retinopathy, retinal vein occlusion, uveitis, and cataract extraction. Although fluorescein angiography is highly sensitive for the qualitative detection of fluid leakage which causes macular edema, measurements of retinal thickening may correlate better with areas of retinal dysfunction than the amount of fluorescein leakage. OCT provides high longitudinal resolution cross-sectional images of retinal structure and direct measurements of retinal thickness are possible from the tomographs. OCT images obtained in patients with cystoid macular edema closely correspond to known histopathology.[68] Measurements of retinal thickness at the same location in tomographs acquired longitudinally over time provide an objective means of tracking the development or resolution of fluid accumulation. Unlike conventional slit-lamp observation or fluorescein angiography, these measurements enable the objective monitoring of disease progression or resolution with a single, permanently recorded number. For example, OCT is useful in quantitatively monitoring retinal thickness changes before and after focal laser photocoagulation treatment for macular edema. In patients with diabetes mellitus, measurements of retinal thickness with OCT in the central fovea correlate with best corrected visual acuity. In a preliminary study, a simple linear regression provided a good fit (adjusted $R^2 = 0.78$) between foveal thickness and visual acuity. In this study, OCT was also more sensitive compared to slit-lamp biomicroscopy to small changes in retinal thickness. These results suggest that OCT is promising as a sensitive diagnostic for macular thickening, the major treatable cause of vision loss in diabetic retinopathy.

OCT also offers an objective test for the quantitative evaluation of patients with central serous chorioretinopathy, a common cause of reduced vision among middle-aged men. Longitudinal examinations with OCT are able to track the resolution of the sensory retinal detachment in this

---

65 C.A. Puliafito, M.R. Hee, C.P. Lin, E. Reichel, J.S. Schuman, J.S. Duker, J.A. Izatt, E.A. Swanson, and J.G. Fujimoto, "Imaging of Macular Diseases with Optical Coherence Tomography (OCT)," *Ophthalmol.,* forthcoming.

66 J.S. Schuman, M.R. Hee, C.A. Puliafito, C. Wong, T. Pedut-Kloizman, C.P. Lin, E. Hertzmark, J.A. Izatt, E.A. Swanson, and J.G. Fujimoto, "Quantification of Nerve Fiber Layer Thickness in Normal and Glaucomatous Eyes Using Optical Coherence Tomography: A Pilot Study," *Arch. Ophthalmol.,* forthcoming.

67 M.R. Hee, C.A. Puliafito, C. Wong, J.S. Duker, E. Reichel, J.S. Schuman, E.A. Swanson, and J.G. Fujimoto, "Optical Coherence Tomography (OCT) of Macular Holes," *Ophthalmol.,* forthcoming.

68 M.R. Hee, C.A. Puliafito, C. Wong, J.S. Duker, E. Reichel, B.K. Rutledge, J.S. Schuman, E.A. Swanson, and J.G. Fujimoto, "Quantitative Assessment of Macular Edema with Optical Coherence Tomography (OCT)," submitted to *Arch. Ophthalmol.*

disease with more sensitivity than slit-lamp biomicroscopy.[69]

Clinical imaging of the optic nerve with OCT is directly relevant to the early diagnosis of glaucoma, the third leading cause of blindness in the U.S. Unlike tonometry, visual field testing, or optic nerve head appearance, OCT images of peripapillary nerve fiber layer thickness may be able to provide an objective early indicator of glaucoma onset. In preliminary studies, OCT images have been correlated with visual field testing and fundus photography in a cross-section of patients.[66] Areas of retinal nerve fiber layer thinning correlate with regions of visual field loss, and the severity of thinning is indicative of the stage of glaucoma. Taken together, these studies suggest that OCT is a promising diagnostic tool in clinical ophthalmology.

1.15.2 In vivo Imaging of Laser-Induced Retinal Lesions Using OCT

An understanding of laser-tissue interaction in the eye is relevant both to laser surgery as well as to establishing standards for laser eye safety. Previous studies which establish laser retinal injury thresholds have been based primarily on ophthalmoscopic or fluorescein angiographic examination of the retina.[70] Histopathology provides direct measurement of the morphology and ultrastructural changes which accompany retinal laser injury.[71] However, this technique requires that a specimen be obtained for microscopic examination.

During the past year, we have taken a new approach to investigating laser retinal injury using optical coherence tomography (OCT). OCT is a new imaging technique which utilizes fiber optic based low-coherence interferometry along with a super luminescent diode laser source to provide micron scale cross-sectional tomographic images of retinal structure. In contrast to conventional histopathology techniques, OCT is noninvasive; therefore, it is possible to image laser induced retinal lesions at different time intervals ranging from immediately after laser exposure to several days. This provides a direct tomographic measurement of the formation and healing response to laser retinal exposure.

Comparative OCT studies were performed at Brooks Air Force Base, Texas, using cw argon, nanosecond, picosecond, and femtosecond laser-induced lesions. Histopathology was acquired at selected time points for comparisons with OCT images. By combining sequentially acquired images, a time-lapse movie illustrating lesion evolution was produced. Additionally, images acquired spatially across the retinal surface, and later assembled, enabled the visualization of the three-dimensional structure of an optic disk.

These studies are the first *in vivo* microstructural measurements which document the formation and healing response of retinal laser exposure, provide improved visualization of retinal structure, and have important implications for ophthalmic laser surgery as well as establishing laser retinal injury standards.

1.15.3 Noninvasive OCT Imaging for Cataract Evaluation

Clinically, the primary means for cataract evaluation is by slit-lamp examination. Although this provides a reasonably adequate view of the lens, the grading of cataract formation is based upon a subjective grading system used by the clinician. A more quantitative means of evaluating the lens is by Scheimpflug imaging. The Scheimpflug camera and anterior eye segment analysis system provide a small margin of error (3-9 percent), but the examiner using this device must be very experienced in order to reproduce clinically viable data.[72] In addition, the instrument is not available to most clinicians.

The use of OCT to image cataracts provides quantitative data of optical reflectance within the lens. Previously in our laboratory, we have imaged

---

[69] M.R. Hee, C.A. Puliafito, C. Wong, J.S. Duker, E. Reichel, J.S. Schuman, E.A. Swanson, and J.G. Fujimoto, "Optical Coherence Tomography (OCT) of Central Serous Chorioretinopathy," *Am. J. Ophthalmol.*, forthcoming.

[70] R. Birngruber, V.-P. Gabel, and F. Hillenkamp, "Threshold Criteria and Derivation of Safe Levels for Laser Radiation," in *Current Concepts in Ergophthalmology*, eds. B. Tengroth, D. Epstein, A. Anseth, A. Hedin, A.H. Keeney, M.J. Roper-Hall, and D.H. Sliney (The Hague, The Netherlands: 1978).

[71] B. Lorentz, "Morphologic Changes of Chorioretinal Argon Laser Burns during the First Hour Post Exposure," *Lasers Life Sci.* 2: 207 (1988).

[72] Y. Sakamoto and K. Sasaki, "Accuracy of Biometrical Data Obtained from the NIDEK EAS-1000," *Ophthalmic Res.* 26 (suppl. 1): 26 (1994).

bovine lenses *in vitro* using OCT after cold-induced cataracts were formed.[63] This year, we completed the first in vivo study using OCT to image lenticular cataracts in a colony of geriatric rhesus monkeys with historically documented radiation-induced cataracts.[73] The documented cataract grading of this colony was accomplished using the subjective grading system and provides complete descriptions of the cataracts that were imaged. Detailed images were produced from 18 subjects with cataracts ranging in grade from 0 to 3. Nuclear, cortical, and subcapsular opacities were clearly imaged in the anesthetized subjects. Each image was produced from an average of three scans with each scan taking 20 s to complete. Movement artifacts were subsequently removed through image processing on a computer. Faster image acquisition will be necessary before images can be obtained in human subjects.

Cataracts with increasingly dense opacities revealed under slit-lamp examination correlate well with the increasing optical reflectance detected with OCT. In addition, OCT was able to detect opacities previously hidden posterior to nuclear opacities. When OCT images were acquired prior to slit-lamp examination, images provided direction toward visually confirming the opacities that were extremely subtle and would have been missed otherwise. These early results suggest that OCT can be readily utilized as a noninvasive means of quantitatively grading cataracts and identifying opacities not easily observed during standard slit-lamp examination.

1.15.4 OCT Enhanced Confocal Microscopy

The axial and lateral resolution of cross-sectional OCT images is increased by combining OCT with confocal microscopy.[74] For OCT enhanced confocal microscopy, the reference arm length is matched to the focus of the high numerical aperture objective illuminating the sample. The sample is scanned axially and laterally through the focus of the objective, and the interferometric signal is detected at every scan position.

OCT enhanced confocal microscopy narrows the system point spread function (PSF) of the confocal microscope by multiplying the PSF defined by the coherence envelope with that of the confocal system. Also, coherent detection limits the multiple scattering contribution to the resultant confocal image. Both improvements enable OCT enhanced confocal microscopy to provide higher resolution and greater contrast than standard confocal microscopy.[74]

The OCT enhanced confocal microscope consists of broad bandwidth superluminescent diode centered at 850 nm. The coherence length of the source is approximately 20 nm. The source is coupled into a single mode fiber-optic Michelson interferometer. The fiber is modulated at 20 KHz with a piezoelectric transducer, and the interference signal is detected using a lock-in amplifier. The heterodyne detection of the OCT enhanced confocal system provides a signal-to-noise ratio in excess of 110 dB. The sample arm objective has a high magnification ranging from 40 to 100 times, and numerical aperture ranging from 0.85 to 1.3. The pinhole of the OCT enhanced confocal system is the aperture of the single mode fiber of the object arm. The image is formed from the magnitude of the interferometric signal detected as the sample is raster scanned through the focus. The total image scan time ranges from 5 to 15 minutes.

OCT enhanced confocal microscopy has been used to image microscopic features of *in vitro* skin lesions. Images obtained from the OCT enhanced confocal microscopy system show cellular morphology up to 200 μm deep. The OCT enhanced confocal images also allow visualization of the dermoepidermal junction and dermal structures. The ability of OCT enhanced confocal microscopy to image cellular and architectural morphology of skin validates the use of this approach for obtaining high resolution optical biopsies.

1.15.5 Optical Biopsy

A cross-sectional optical imaging device for performing noninvasive "optical biopsies" in human tissue would greatly improve the quality of medical care. The optical biopsy might be done by cross-sectional imaging of backscattered reflectance from architectural and cellular structures within tissue.

---

[73] A.B. Cox et al., "Progress in the Extrapolation of Radiation Cataractogenesis Data Across Longer-Lived Mammalian Species," in *Biological Effects and Physics of Solar and Galactic Cosmic Radiation,* Part A, eds. C.E. Swenberg et al. (New York: Plenum Press, 1993).

[74] J.M. Schmitt, A. Knuttel, A. Gandjbakche, and R.F. Bonner, "Optical Characterization of Dense Tissues using Low-Coherence Interferometry," *SPIE* 1889: 197 (1993); J.A. Izatt, M.R. Hee, and G.M. Owen, "Optical Coherence Microscopy in Scattering Media," *Opt. Lett.* 19: 590 (1993).

Cross-sectional reflectance images could have functional as well as structural significance if the wavelengths were selected around absorption maxima of endogenous chromophores that are physiologically significant, e.g., hemoglobin. Measuring spatially localized reflectance in tissue is complicated by multiple scattering, however. Optical coherence tomography (OCT) is a new technique that uses low coherence interferometry to gate out multiply scattered photons and produce cross-sectional reflectance images.

An OCT system that accommodates multiple sources has been constructed. The source is coupled into a single mode optic based Michelson interferometer. Tissue axial reflectance is obtained by varying the reference arm length and digitizing the magnitude of the demodulated interference envelope. A cross-sectional image is produced by recording axial reflectance profiles while the tissue specimen is scanned laterally.

Clinically relevant OCT images of pathologic *in vitro* human tissue have been obtained using superluminescent diodes at two different wavelengths, 850 and 1300 nm. For both wavelengths, the system has an axial resolution of approximately 20 μm, object arm power of 100 μW, and a signal-to-noise ratio (SNR) of 100 dB. Reflectance images of coronary artery and aortic atherosclerotic plaques demonstrate a clear delineation between cardiac muscle, fatty plaque, and fibrous tissue. Architectural morphology of normal and pathologic *in vitro* human tissue specimens, including skin, lung, respiratory tract, gastrointestinal tract, bone, and cartilage have also been imaged. OCT imaging at 1300 nm has been found to be superior to 850 nm because of increased penetration depth. The variation in penetration is likely due to the decreased attenuation from tissue scattering and absorption at 1300 nm.[75]

A wavelength tunable modelocked Kerr lens modelocked Ti:Al_2O_3 laser has been constructed for coupling into the OCT system. Ultra high axial resolution (<4 μm) OCT images from aortic atherosclerotic plaques and other human tissues have been acquired using the Ti:Al_2O_3 laser. Our studies show that ultra high resolution OCT images obtained using the Ti:Al_2O_3 laser are superior to images produced by the SLD based systems.

The Ti:Al_2O_3 laser allows samples to be illuminated by more than 50 mW of optical power distributed over the wide spectral range of 750-875 nm. The ultra high resolution OCT system has greater resolution than the SLD based systems because of the large spectral bandwidth, and accompanying shorter coherence length of the Ti:Al_2O_3 laser. In addition to providing a large dynamic range (115 dB), the high power of this source permits rapid image acquisition. The wavelength tunability of the Ti:Al_2O_3 laser also has applications for performing research on the optical properties of tissue. Future studies will be conducted using this laser to perform OCT spectroscopy of human tissue.

Our lab has demonstrated the use of OCT for noninvasive diagnostic imaging of human tissue. OCT images at 1300 nm contain more diagnostic information because of increased penetration depth. The high resolution of the Ti:Al_2O_3 OCT system outperforms SLD based systems for imaging tissue architectural morphology. These studies suggest that OCT and ultra high resolution OCT will become important tools for performing noninvasive "optical biopsies" in the future.

1.16 EUV Laser Studies

Sponsor

MIT Lincoln Laboratory
Contract BX-5098

Project Staff

Professor Peter L. Hagelstein, James G. Goodberlet, Timothy A. Savas, Marc Fleury, Martin H. Muendel, Sumanth Kaushik

In previous RLE reports, we have described our progress toward the development of small scale EUV lasers at MIT. In this report, we provide a brief overview of results and goals.

Our basic approach is to ionize the surface of a solid flat target with a pump laser pulse (about 1 J in 60 ps) in-line focus to produce a hot low-density plasma. The plasma length is up to about 1 cm, the laser focus is about 30 microns, and the low-density plasmas of interest for EUV laser studies are formed from 100 to 500 μ above the target surface. In the collisional scheme, direct collisional excitation of the ground state of the Ni-like ions produces a population inversion between the excited state n=4 levels; we have observed amplifi-

[75] J.M. Schmitt, A. Knuttel, A. Gandjbakche, and R.F. Bonner, "Optical Characterization of Dense Tissues using Low-Coherence Interferometry," *SPIE* 1889: 197 (1993); J.M. Schmitt, A. Knuttel, M. Yadlowsky, and M.A. Eckhaus, "Optical Coherence Tomography of a Dense Tissue: Statistics of Attenuation and Backscattering," *Phys. Med. Biol.* 39: 1705 (1994).

cation on the 4d-4p transition in Ni-like Nb at 204 Å. In the recombination scheme, a population inversion is produced when electrons recombine onto ions in a cooling plasma; we have observed amplification of the 3d-2p transition in H-like B at 262 Å.

Considerable development of our system during the past year has given us a new capability for short pulse and long pulse operation; we have further developed our diagnostics, improving sensitivity using a microchannel plate imaged onto film.

Preliminary experiments using the new system indicate that recombination experiments appear to achieve better ionization with longer pulses. The collisional schemes have been predicted to work better with shorter pulses at high intensity, but this has not yet been tested. There is reason to believe that the use of short pulses for these schemes will produce an underionized plasma. New experiments to clarify these issues are ongoing.[76]

1.16.1 Pulse Compression System

The electron collisional EUV laser schemes are pumped more efficiently the hotter the electron distribution; consequently, an increase in the pump intensity will result in an increased electron temperature. One approach to this is to employ a larger pump laser capable of a higher pump power; this approach has been demonstrated to work at laser facilities that can deliver more energy than ours by a factor of 1000. We decided instead to pursue the use of a higher intensity pump pulse which we obtained by implementing a pulse compression scheme into our pump laser system.

The compression system is shown in figure 6. The system employs chirped-pulse amplification, based upon bulk glass self-phase modulation, to generate shorter pump pulses at higher peak power. In order to increase the pulse bandwidth, the amplified oscillator pulse of 60 ps is focused into bulk SF6 glass, $n_2 = 9 \times 10^{13}$ esu in a double pass optical arrangement. The spectrally broadened pulse is temporally stretched with a grating pair pulse stretcher to 120 psec, limited by the nonlinear phase modulation of the glass. The stretcher consists of two 1800 lines/mm gratings separated by three meters and an inverting lens pair; the beam makes two passes through the stretcher.

The 120 ps pulse is amplified by passing through the zig-zag slab power amplifier, and then shortened to 20 ps by a second 1800 lines/mm grating pair compressor. The compressor gratings are used 8° off Littrow and separated by seven meters; the transmission efficiency of system from slab amplifier to target was meaured to be 67 percent. We are presently able to pump at 800 mJ with 20

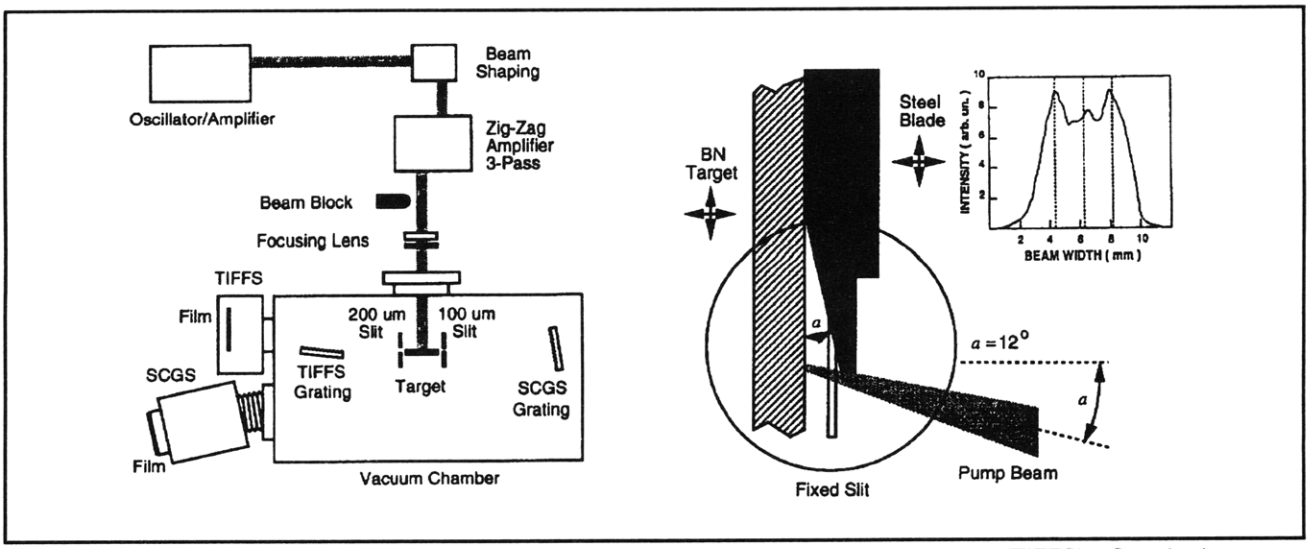

Figure 6. (a) The MIT table-top x-ray laser system. Time integrated flat field spectrometer (TIFFS). Streaked concave grating spectrometer (SCGS). (b) Target and blade arrangement used for H-like recombination laser. Insert: Transverse intensity profile of pump-laser beam.

---

[76] P.L. Hagelstein, J. Goodberlet, M. Muendel, T. Savas, M. Fleury, S. Basu, and S. Kaushik, "Recent Progress in Table-Top Lasers at MIT," *Proceedings of the International Symposium on X-ray Lasers,* Williamsburg, Virginia, June 1994; J. Goodberlet, T. Savas, S. Basu, M. Muendel, S. Kaushik, M. Fleury, and P.L. Hagelstein, "Recent Experiments with the MIT Table-Top X-ray Laser System," *Proceedings QELS,* Quebec, 1994.

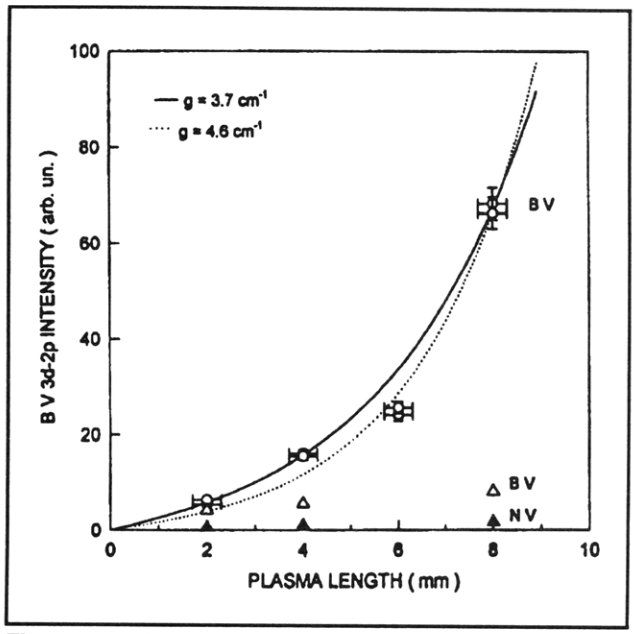

Figure 7. Line intensities, recorded with the SCGS, for several plasma lengths. 400 μm above the target surface, the B V 3d-2p line, shown as circles, exhibited amplification. 250 μm above the surface, the B V line showed optically thick behavior and the N V 3s-2p line showed linear growth.

ps pulses, and 1.5 J with 120 ps pulses; increasing the bandwidth further (which is planned for the near future) will allow us to pump with 1.5 J at 15 ps, and 3 J at 220 ps.

1.16.2 Short-Pulse Versus Long-Pulse Plasma Heating

While it is expected theoretically that pumping with a higher intensity will produce an increased coronal electron temperature, this effect can be mitigated to some degree by an increased PdV cooling rate. Use of an intense short pulse should produce higher gain in the collisional scheme, as long as Ni-like ions are present when the intense pulse arrives. There has been concern as to whether a short intense pulse can produce the proper conditions for EUV lasing.

Experiments were carried out to examine the response of the coronal plasma to laser pulses of different intensities. Carbon and boron plasmas were studied comparing 20 ps and 120 ps single pulse irradiation at constant energy; carbon plasmas were studied at 1 mm and 4 mm length, and boron plasmas were studied at 8 mm. The experiments indicated stronger 2p-1s and 3d-2p emission at 120 ps, and stronger H-like to He-like K-shell emission, apparently consistent with the production of a hotter coronal plasma at the longer pulse length.

If the electron temperature goes down more rapidly by PdV cooling in the case of short-pulse pumping, then the use of two-pulse irradiation should reduce the PdV cooling during the second pulse since the plasma is pre-expanded. The results of the two-pulse measurements in a carbon plasma showed an improvement in the short-pulse emission, but the long-pulse irradiation results in a "hotter" spectra. Experiments to explore plasma heating in calcium plasmas are ongoing (Ne-like calcium is an EUV laser candidate that may be within our range).

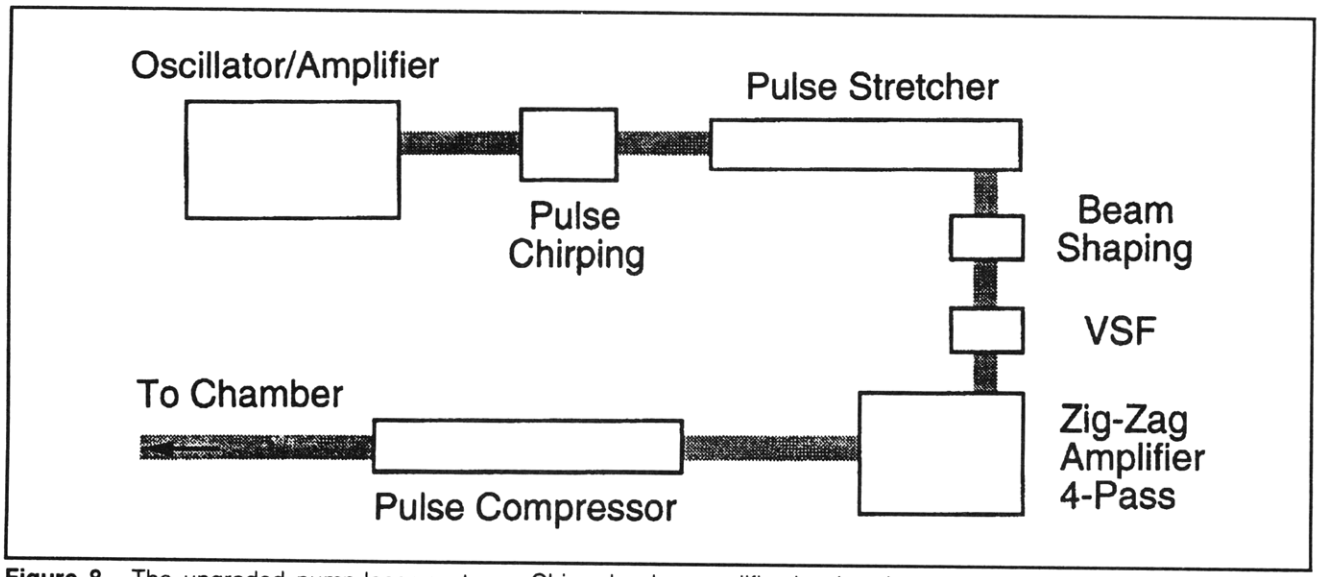

Figure 8. The upgraded pump-laser system. Chirped pulse amplification has been on the pump-laser system. The pulse is chirped in bulk SF6 glass, and is stretched and compressed with two grating pairs. VSF: Vacuum spatial filter.

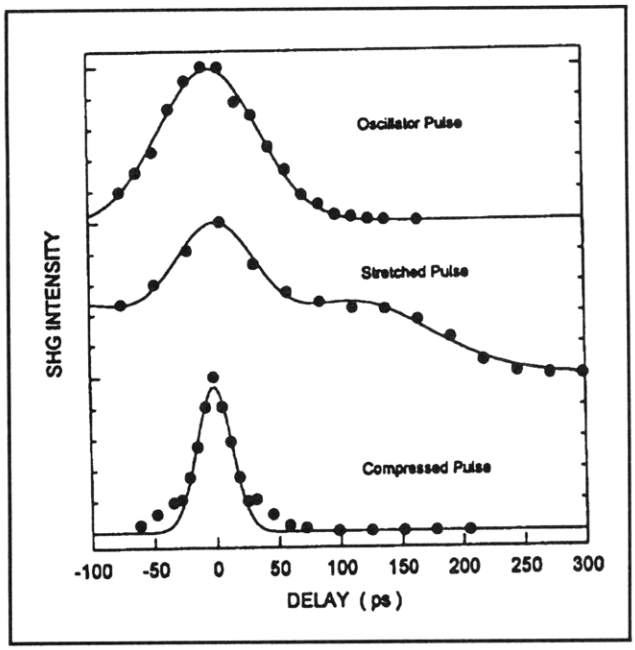

Figure 9. Second harmonic generation pulse measurements. The oscillator pulse, stretched pulse and compressed pulse durations were found to be 62 ps, ~ 120 ps, and 20 ps, respectively.

1.16.3 EUV Diagnostics Upgrades

As described in previous reports, we have fielded two EUV diagnostics. The primary spectrometer diagnostic has used a nearly stigmatic concave spherical grating at near normal incidence to image onto an x-ray streak camera. The secondary spectrometer has used a flat-field variable spacing Harada grating that has imaged onto a microchannel plate or directly onto film. Experience with both diagnostics has indicated that our experiments would be accelerated and improved by some modifications, which are described below.

The use of the Harada grating spectrometer has provided important x-ray spectra below 100 Å, but as implemented, a break in the vacuum was required to recover film. An insert was designed, built, and implemented in order to speed this up by an order of magnitude. The use of a microchannel plate detector at the Harada image plane will allow us to extend this range to 450 Å, to relay the image out of the vacuum chamber, while retaining spatial information. The Harada spectrometer has the potential to detect beam formation that would allow single shot gain analysis.

We have implemented a microchannel plate detector at the image plane of the concave grating spectrometer for time-integrated imaging. This has resulted in a doubling of the available spectral range; it has increased the sensitivity of the diagnostic and extended our spectral range: we can now measure from 140 Å to 420 Å. A set of experiments can now be recorded on a single piece of film, increasing the shot rate and reducing film costs. The film response can be avoided now by capturing the microchannel plate image with a CCD array. The spectrometer now gives us spatial information about the plasma emission; the H-like boron 3d-2p emission is observed to be localized within a 200 x 400 μ region above the target. The cooling of the plasma by blades placed in the coronal region is now readily apparent in the 2D images.

1.16.4 Shallow-angle Pumping Experiments

While side-pumped EUV lasers have been demonstrated at a number of laboratories and have also played an important role in the development of the field of short wavelength lasers, side-pumped plasma targets have not produced particularly efficient EUV lasers. The highest conversion efficiencies observed so far are 10^{-5}, as determined by the ratio of output energy to input laser pump energy.

An improvement in overall efficiency is expected through the use of end-pumping in pre-expanded plasmas. Much of the inefficiency of current short wavelength lasers occurs because: (1) high density plasma is heated and not used; (2) much of the absorbed energy goes into accelerating plasma; (3) in some target arrangements, the absorbed energy is not large. In the next section, we discuss further our efforts to develop a low density end-pumped gaseous laser.

We pursued shallow-angle pumping of slab targets as a possible route to more efficient EUV lasers. The basic idea is that a beam incident at shallow angle is turned at low density, so that only low density plasma is heated. While most of the beam is not absorbed, it can in principle be used again by refocusing. In order to obtain a profile suitable for EUV laser experiments, a prepulse is required.

In a preliminary set of experiments, shallow-angle pumping was attempted in H-like B coronal plasmas. We were able to produce a line focus by transverse irradiation and then bring a second beam in at glancing angle to heat the pre-formed coronal plasma. As the constraints on relative alignment were rather stringent, it was important to prove that the shallow angle beam in fact hit the plasma region. Observations of the shallow-angle beam emerging from the plasma showed that the coronal plasma refracted the incident beam, in some cases causing beam break-up.

One potential advantage of shallow angle pumping is the increase in pump intensity that occurs. In

these experiments, a pump intensity of 3 x 10^{13} Watts/cm^2 was demonstrated, as compared to a transverse pump intensity of 10^{13} Watts/cm^2. In these experiments, the Harada grating spectrometer was used with film, and the x-ray lines below 60 Å were monitored.

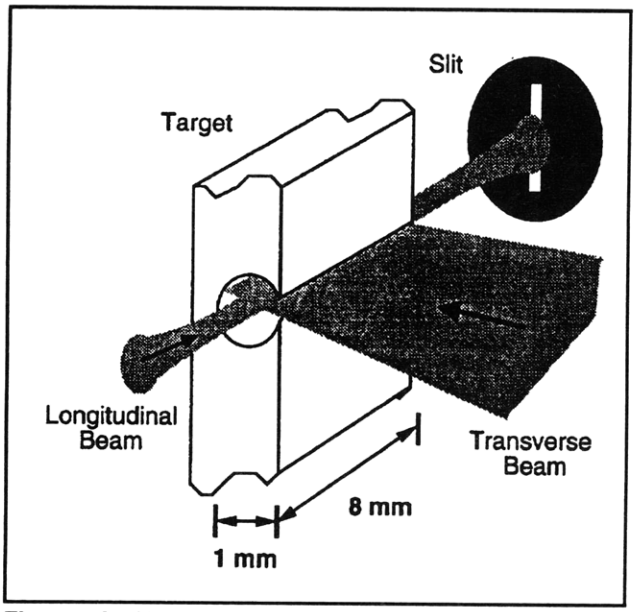

Figure 10. New pumping arrangement. Transverse- and longitudinal-pumping was imlemented with a new target geometry. The solid BN target was designed to counter effects of beam refraction.

1.17 Collisional and Recombination Schemes at Longer Wavelength

Sponsor

MIT Lincoln Laboratory
Contract BX-5098

Project Staff

Professor Peter L. Hagelstein, James G. Goodberlet, Timothy A. Savas, Marc Fleury, Martin H. Muendel, Sumanth Kaushik

Experiments on small scale systems have recently achieved some successes at other laboratories. Midorikawa and coworkers claim to have seen significant gain in H-like Li near 135 Å, in a recombining plasma created by optical field ionization from an intense femtosecond pulse.[77] Rocca and colleagues have recently obtained up to seven gain lengths in Ne-like argon at 469 Å in capillary discharge experiments[78] and the Stanford group has recently obtained 11 gain lengths gain in Pd-like Xe at 418 Å, using optical field ionization with a circularly polarized femtosecond pulse.[79]

So far, we have explored the Ni-like collisional scheme in Nb at 204 Å,[80] and the H-like recombination scheme in B at 262 Å.[81] The peak gain in these experiments corresponds to 2.2 and 3.0 gain lengths as interpreted conservatively using the Linford formula. The Linford formula assumes an angular resolving diagnostic, while our diagnostic was angle-integrating; correcting for this effect would lead to about 3 and 4 gain lengths in the two sets of experiments.

Recently, we have been considering different strategies in order to improve on the total number of gain lengths. We have modified our system to be able to use shorter pulses in order to achieve a higher intensity (and thus higher temperatures) in the collisional schemes. Using longer pulses appears to help the recombination schemes. The recombination scheme takes advantage of a blade[82] to improve cooling; we experimented with many different blade configurations. Some exploratory end-pumped and shallow-angle pumped experiments were done, primarily with the boron recombination scheme.

---

[77] Y. Nagata, K. Midorikawa, S. Kubodera, M. Obara, H. Tashiro, and K. Toyoda, "Soft X-ray Amplification of the Lyman-α Transition by Optical Field-induced Ionization," *Phys. Rev. Lett.* 71: 3774 (1993).

[78] J.J. Rocca, V. Shlyaptsev, F.G. Tomasel, O.D. Cortazar, D. Hartshorn, and J.L.A. Chilla, "Demonstration of a Discharge Pumped Table-Top Soft-X-ray Laser," *Phys. Rev. Lett.* 73: 2192 (1994).

[79] B.E. Lemoff, G.Y. Yin, C.L. Gordon III, C.P.J. Barty, and S.E. Harris, submitted to *Phys. Rev. Lett.*

[80] S. Basu, P.L. Hagelstein, J.G. Goodberlet, M.H. Muendel, and S. Kaushik, "Amplification in Ni-like Nb at 204.2 Å Pumped by a Table-top Laser," *Appl. Phys. B* 57: 303 (1993).

[81] J. Goodberlet, S. Basu, M.H. Muendel, S. Kaushik, T. Savas, M. Fleury, and P.L. Hagelstein, *J. Opt. Soc. Am. B*, forthcoming.

[82] D. Kim, C.H. Skinner, G. Umesh, and S. Suckewer, "Gain Measurements at 18.22 nm in C VI Generated by a Glass Laser," *Opt. Lett.* 14: 665 (1989).

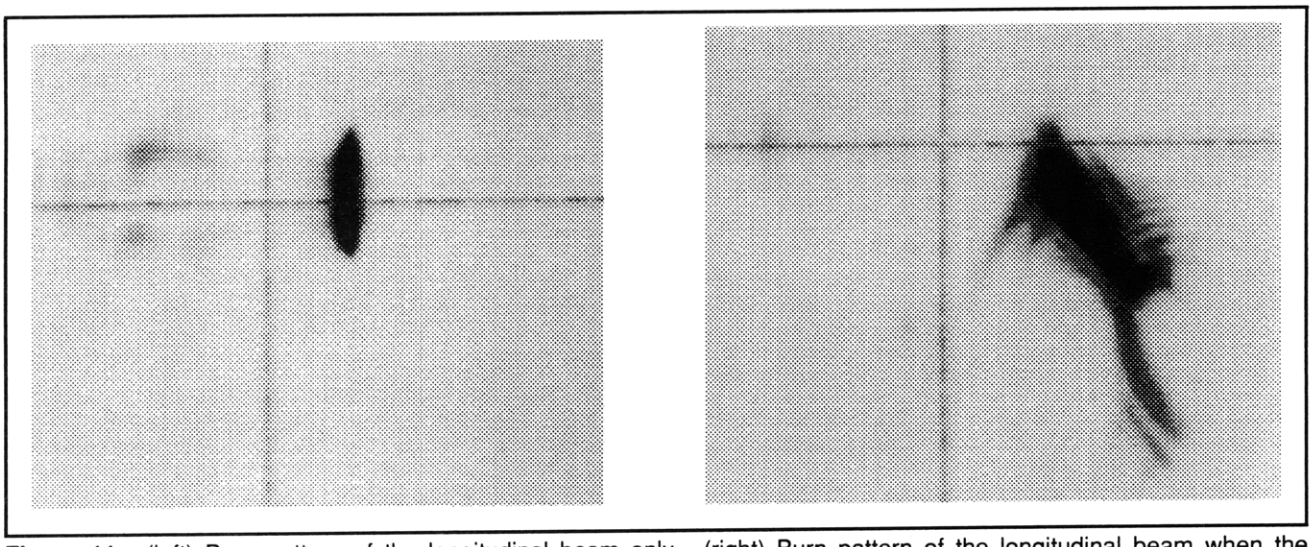

Figure 11. (left) Burn pattern of the longitudinal beam only. (right) Burn pattern of the longitudinal beam when the transverse beam is allowed to preform the plasma. Beam break-up, due to the plasma, is evident.

Longer wavelength schemes should require less pump power. Consequently, we have been considering different classes of schemes at longer wavelength. As our best results to date have been in the recombination scheme, we consider extensions of this scheme in other sequences first. In table 1 we show recombination schemes in the various alkali-isoelectronic sequences with predicted pump intensities that are less than the pump power for H-like B. While the Li-like scheme has been studied for many years (primarily Li-like Al), only recently has some work been reported in the Na-like scheme; no work has been reported in Cu-like ions yet.

It is expected that these recombination schemes will suffer from radiation trapping. Perhaps coincidentally, it has been found to be very difficult to obtain a large gain length product on these transitions in other ions. There exists a class of recombination schemes which would not be expected to suffer such a large trapping effect. Schemes that are available at our pump intensities are listed in table 2. High gain was observed in Li-like S on such a transition.

Table 1. Accessible recombination schemes. λ is the laser wavelength, ΔE is the ionization energy of the ground state electron, I_{est} is the predicted incident pump intensity.

Sequence	Element	Transition	λ (Å)	ΔE (eV)	$I_{est}\left(\frac{W}{cm^2}\right)$
H-like	B	3d-2p	262	340	1.2×10^{13}
Li-like	F	4f-3d	382	167	4.1×10^{12}
Na-like	Ca	5g-4f	402	151	3.6×10^{12}
Na-like	Ti	5g-4f	279	218	6.2×10^{12}
Cu-like	Mo	6h-5g	380	167	4.1×10^{12}

Table 2. Accessible Untrapped Recombination Schemes.

Sequence	Element	Transition	λ (Å)	ΔE (eV)	$I_{est}\left(\frac{W}{cm^2}\right)$
Li-like	Mg	5g-4f	404	340	1.2×10^{13}
Na-like	Cr	6h-5g	380	296	9.8×10^{12}
Cu-like	Pd	7i-6h	382	275	8.8×10^{12}

Collisional excitation schemes at longer wavelength are also of interest, especially given the recent results in Ne-like A by Rocca and coworkers. While the density and temperature required for argon match our plasmas rather well, it is not easy to use argon in our experiments. As the odd Z versions of the scheme have substantially reduced gain due to hyperfine broadening, the next available scheme is Ne-like Ca. According to the intensity requirements, calcium may be out of our reach. Some preliminary experiments with Ca have been done,

but no gain has been seen. The Ni-like schemes at longer wavelength require a lower pump intensity, but the gain is predicted to be correspondingly lower (due to operation at lower electron density). Our previous efforts at pumping Ni-like Zr were hindered also by the presence of strong emission due to oxygen contamination. Also of interest are higher Z collisional schemes, like the Pd-like ions (demonstrated at Stanford) and the Nd-like ions. While the Nd-like ions that are accessible are unlikely to produce gain, due to a poor ratio of radiative decay rates, it is probable that the Pr-like ions near Z=80 would show gain.

Table 3. Accessible Collisional Schemes.

Sequence	Element	Transition	λ (Å)	ΔE (eV)	$I_{sat}\left(\frac{W}{cm^2}\right)$
Ne-like	Ca	3p-3s	390	405	1.6×10^{13}
Ni-like	Sr	4d-4p	267	195	5.2×10^{12}
Ni-like	Y	4d-4p	242	222	6.4×10^{12}
Ni-like	Zr	4d-4p	221	250	7.6×10^{12}
Pd-like	La	5d-5p	304	~200	$\sim 5.5 \times 10^{12}$

1.18 Toward a Novel End-Pumped EUV Laser

Sponsor

MIT Lincoln Laboratory
Contract BX-5098

Project Staff

Marc Fleury, Professor Peter L. Hagelstein, James G. Goodberlet, Martin H. Muendel

Most laser-driven short wavelength lasers that have been studied make use of plasmas that are created from solid surfaces or thin films by pumping from the side. The efficiencies that have been obtained using this approach have been low; the best efficiencies reported to date have been on the order of 10^5 for side pumping.

There are many reasons for this. Ablation from a solid surface leads to heating of unwanted high density plasma, large conduction losses, and significant hydrodynamic losses. Laser-heating of thin foils leads to similar losses, but also leads to very a low absorption efficiency when the foil has expanded to low density.

Many of these problems can be overcome through the use of end-pumping of a pre-expanded low density plasma. The end-pumped beam will be absorbed efficiently in passing through a long low density plasma, as long as it can stay within the plasma. If the plasma is pre-expanded, the hydrodynamic losses will be minimized. The use of a low density plasma increases the efficiency of the population kinetics. Such systems have the potential to reach an efficiency of on the order of 10^{-2}. Successful implementations of low energy femtosecond EUV laser pumping schemes have to date been all end-pumped lasers.

Recently, Milchberg and coworkers have demonstrated a plasma channel that works as an optical fiber for pump radiation.[83] This is important since the ionization of the plasma typically results in defocusing and beam break-up. Milchberg et al. used a transmitting axicon to create a plasma channel, and then demonstrated stable beam propagation within the channel.

The length of the channel in this work was limited by the high power requirements for channel formation. We have proposed to employ a reflecting tube to refocus the light from the axicon in order to obtain a longer channel.[84] This is illustrated in figure 12.

This design is the combination of an axicon (conical part) and a tube; it can be thought of as an 'optical funnel'. The axicon focuses a collimated beam down to a line on its axis and the tube refocuses this line again and again down its length. This scheme is exact since from the side-view it can be seen that the axicon focuses down to its center and the tube re-focuses on the same point translated. The dimensions are such that each re-focus matches the end of the previous one thereby creating a continuous line focus.

The constraints on this piece are quite stringent. The surface quality must be as good as those of mirrors for high powered lasers. The constraints on the figure of the piece are dictated by the necessity to have a tight focus on axis and a straight line by exact refocusing. That is to say that the piece

[83] C.G. Durfee III and H. Milchberg. "Light Pipe for High Intensity Laser Pulses," *Phys. Rev. Lett.* 71: 2409 (1993).

[84] P.L. Hagelstein, J. Goodberlet, M. Muendel, T. Savas, M. Fleury, S. Basu, and S. Kaushik, "Recent Progress in Table-Top Lasers at MIT," *Proceedings of the International Symposium on X-ray Lasers*, Williamsburg, June 1994.

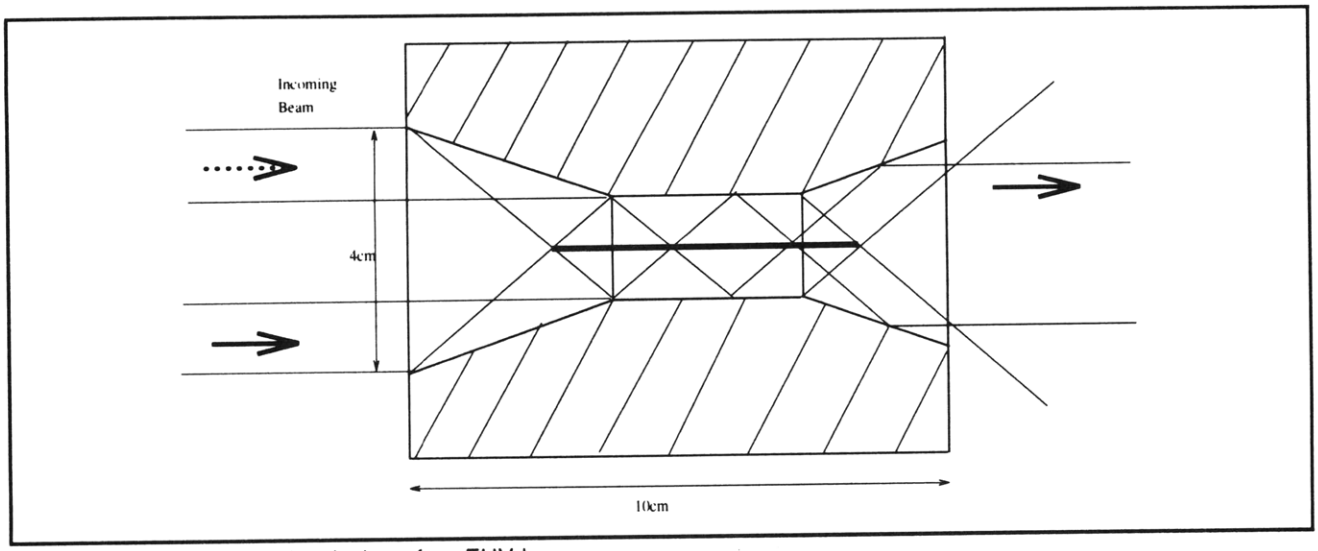

Figure 12. Axicon and tube design of an EUV laser.

needs μm-precision over 20 cm. These optics can be fabricated using hard diamond-turning of OFHC copper, a technology developed over the last 10 years. A mock version of this mirror in brass has been machined and polished here at MIT (figure 13).

We have studied the focusing properties of the mock-up axicon and tube. Refocusing has been demonstrated over a length of 20 cm. On center, an amplification factor of 1200 in a diameter of 80 μm has been recently measured by scanning the intensity profile.

Figure 13. Scattering of He-Ne light from condensation at the focus of the mock-up axion and tube.

1.19 Photon Operators and Photon Configuration-Space Equations

Project Staff

Professor Peter L. Hagelstein

In a number of recent publications on pulse propagation in fibers, the description of the radiation field has been cast in terms of second quantized photon operators. This is unusual, since quantum radiation theory is usually cast in terms of field operators ($\hat{E}$, $\hat{H}$, or $\hat{A}$ operators), and most problems are worked out in terms of these field operators.

The photon operators are quite interesting for several reasons. One can compute the field distributions, the energy distribution and the photon distribution; if you do, you will find the photon distribution does not coincide with the energy distribution. A gedanken box could be constructed inside of which a photon is localized; it would be found that the associated fields extend outside of the box. Another gedanken box could be constructed to contain the electric and magnetic fields associated with a photon; yet it can be shown that the associated photon will not be localized within that same box.

Interactions of photons and matter are mediated in QED through the vector potential operator. Written in terms of the vector potential operator, the inter-

action is local; written in terms of the photon field operator, the interaction is fundamentally nonlocal.

QED is a quantum field theory, and as such is cast in terms of field theory operators that are second quantized (they are written in terms of operators that create or destroy photons or electrons). Historically, there has been a considerable computational advantage if a configuration space (first quantization) model is available. An example of this is in atomic structure calculations; the underlying model is QED (a field theory in second quantization), but numerical computations are usually done with the relativistic Hartree-Fock equations which are configuration space equations.

One advantage of studying the photon field operators and their dynamics is that the methods used to obtain configuration space equations from the field theory require a description of the problem in terms of the photon operators. We have recently applied these methods to the second quantized linear response photon Hamiltonian and have derived configuration space equations for photons.[85] Such equations might be termed "Maxwell-Fock" equations, and the single photon equations are very closely related to Maxwell's equations.

For example, the Maxwell-Fock equations for two photons in a dielectric medium would be written in the form:

$$\varepsilon_{aa}\phi_a(r_1) = \alpha_1 \bullet cp_1\phi_a(r_1) + \int U(r_1, s_1)\phi_a(s_1)d^3s_1 - \varepsilon_{ab}\phi_b(r_1)$$

$$+ \int\int\int \phi_b^*(r_2)V(r_1, r_2, s_1, s_2)[\phi_a(s_1)\phi_b(s_2) + \phi_b(s_1)\phi_a(s_2)]d^3r_2\, d^3s_1\, d^3s_2$$

In this equation, the orbitals ϕ are 6 x 1 column vectors, corresponding roughly to three electric field pieces on top of three magnetic field pieces. The $\alpha \bullet cp$ term is a spin-1 analog of the Dirac kinetic energy term; it can be written out in terms of two curls. The dielectric response of the medium is contained in the U terms, and the medium nonlinearity is contained in the photon-photon interaction terms containing V.

In free-space, the 1-photon configuration space equations are mathematically equivalent to Maxwell equations. In the photon equivalent of the Furry picture, the resulting 1-photon configuration space equations are again equivalent to Maxwell's equations in a dielectric medium (which apparently may be nonlocal). The 1-photon results establish the cleanest connection between QED and classical Maxwell equations and under certain restrictions permit Maxwell's equations to be interpreted directly as quantum mechanical equations.

The photon-photon interactions are nonlocal. Photons interact with matter through fields, whose distributions do not correspond to the photon distributions; this results in a nonlocal photon-photon interaction. In a nonlinear medium, the interaction can be attractive, and photons can bind together to form pulses. In first quantization, these pulses are mathematically similar to nuclei. A nucleus has a center of mass, and the nucleons are correlated within fermis of the center of mass. The nuclear center of mass travels through space freely in the absence of potentials; the relative coordinates are used to develop the nuclear states. Analogously, in a nonlinear optical medium, the photonic center of mass will propagate freely in the absence of a spatially varying dielectric medium, and the relative coordinates may be used to build up the photonic internal states.

Interference effects are known for many-particle systems. The center of mass coordinate of atoms can exhibit interference in a two-slit type of experiment. This interference will be preserved as long as the internal state is not altered. Analogously, it would be expected that the photonic center of mass coordinate should be able to exhibit interference effects, as long as the internal photonic state is not altered. This effect is presently unknown exper-

[85] P.L. Hagelstein, "Many-Photon Configuration Space Equations," submitted to *Phys. Rev. A.*

imentally. It would be quite interesting, as the center of mass momentum would be approximately the sum of all the individual photon momenta individually; consequently, the wavelength of the center of mass would be of the order of λ/N, where N is the number of photons. The resulting interference pattern would differ from normal one photon interference patterns.

This new effect is predicted to occur in nonlinear optical media under specialized conditions; it has never been observed and may prove to be difficult to observe. If it can be observed, the effect would be very sensitive to perturbations of the optical material, might serve as a new interferometric optical materials diagnostic, and might have other applications as well. We had examined these pulses initially for their potential to serve as the basis of an optical quantum computer.

In any event, we must be able to observe the effect for it to have any applications. In the future, our interest will be toward understanding the new correlated states predicted by this theory and under what conditions the states can be observed.

1.20 Neutron Hopping

Sponsors

Electric Power Research Institute
Contract RP3170-25
ENECO

Project Staff

Professor Peter L. Hagelstein, Sumanth Kaushik

Electrons are known to hop in solid crystalline materials. Models for electron hopping in ordered and disordered solids have been studied for several decades. Over a wide range of materials and conditions, quantitative models are available that can explain experimental observations. We have recently adapted one such model to the problem of neutron hopping in crystals and have found that a neutron analog to electron hopping should occur.[86]

The existence of a neutron hopping effect is not accepted by many, largely because neutrons are so deeply bound, and because the neutron orbitals are so closely localized around their parent nucleus. If these reasons were not sufficient, then there is the absence of experimental observations of effects that could be attributed to a neutron hopping effect.

Electrons hop due to a first order Coulombic coupling of electron orbitals at a site with orbitals at neighboring sites. Since bound neutron orbitals do not extend to neighboring sites, there is no analogous first order coupling. Nevertheless, there does exist a strong-force mediated coupling between bound neutrons and continuum neutrons, which leads to a weak second-order coupling between bound neutron orbitals at different sites. Brillouin's Theorem would force this coupling to be zero in a fixed core Hartree-Fock approximation. But nucleon-nucleon correlation is very strong in nuclei, so that strong core relaxation effects are present that lead to large residual coupling matrix elements.

This interaction can be described mathematically in terms of a neutron mixed valence Hamiltonian[87]

$$\hat{H} = \sum_{k,\sigma} \varepsilon_k \hat{c}^{\dagger}_{k,\sigma} \hat{c}_{k,\sigma} + \sum_{i,\sigma} \varepsilon_d \hat{d}^{\dagger}_{i,\sigma} \hat{d}_{i,\sigma} + \frac{1}{2} U \sum_{i,\sigma} \hat{n}_{i,\sigma} \hat{n}_{i,-\sigma}$$

$$+ \frac{1}{\sqrt{N}} \sum_{i,k,\sigma} [V_k e^{-ik \cdot \hat{R}_i} \hat{c}^{\dagger}_{k,\sigma} \hat{d}_{i,\sigma} + V^{*}_k e^{ik \cdot \hat{R}_i} \hat{d}^{\dagger}_{i,\sigma} \hat{c}_{k,\sigma}]$$

86 P.L. Hagelstein and S. Kaushik, "Neutron Transfer Reactions," *Proceedings of ICCF4*, Maui, Hawaii, December, 1993; S. Kaushik and P.L. Hagelstein, "A Mixed Valence Model for Second Order Mixing of Neutron Orbitals in a Lattice," *Bull. Am. Phys. Soc.* 40: 317 (1995); P.L. Hagelstein and S. Kaushik, "Possibility of Neutron Hopping in Crystalline Silicon," submitted to *Phys. Rev. B.*

87 P.L. Hagelstein and S. Kaushik, "Neutron Transfer Reactions," *Proceedings of ICCF4*, Maui, Hawaii, December, 1993; P.L. Hagelstein and S. Kaushik, "Possibility of Neutron Hopping in Crystalline Silicon," submitted to *Phys. Rev. B.*

This equation is mathematically closely related to the periodic Anderson model, but the underlying physics is very different. The Anderson model was developed to describe localized states embedded in a continuum; the neutron valence levels are separated from the continuum by several MeV.

We have analyzed this model in the case of a thermal silicon lattice. The results of this analysis indicate that a weak neutron hopping effect is present at high temperature.[88] The basic effect comes about through interaction of the bound neutron orbitals with free Bragg orbitals in the zero-phonon exchange limit. The different Bragg orbitals destructively interfere, and so the effect is maximized through reducing the number of Bragg orbitals that participate. As phonons are exchange more readily at high temperature, the neutron recoil couples to fewer Bragg states at high temperature. There is no analog of this for electrons (since electrons are so light), and we recover an unusual coherence effect that is predicted to improve with increasing temperature.

The silicon lattice has a diamond structure, which is composed of two interpenetrating fcc sublattices. Virtual neutrons originating from one sublattice are predicted to be resonantly Bragg scattered by the other sublattice and delocalized. This leads to a finite site-to-site coupling, which results in a weak temperature-dependent band shift (predicted to be too weak to be observable). The delocalization of the neutron orbitals leads to the possibility of neutron capture at other sites. In natural silicon, this effect would lead to gamma emission at 2.1 MeV due to neutrons originating from ^{29}Si being absorbed by ^{29}Si, at a rate that is too slow to be observable.

The effect is predicted to be stronger for lighter nuclei with outer s-wave valence neutrons, or for strongly driven phonon fields. Phonons exchange through recoil more readily when phonons are already present; this effect is enhanced when a very large number of phonons are in a few modes. Consequently, we anticipate that second order gamma emission at 2.1 MeV should be more readily observable in a driven silicon lattice. Calculations of this effect are in progress.

1.21 Possible Phonon Laser Driven by Exothermic Desorption

Sponsor

Electric Power Research Institute
Contract RP3170-25

Project Staff

Professor Peter L. Hagelstein

We have been interested for some time in the transfer of energy from a lattice to atoms and electrons within the lattice. As is well-known, there are two fundamental modes of energy transfer: energy may be exchanged through (1) the creation and destruction of phonons; and (2) the frequency-shifting of phonons present in the lattice. Energy exchange by frequency shifting in molecular physics is known as the Duschinsky effect; in lattices it has no special name, but the effect is present in the Mossbauer effect (it determines the underlying shape of the Mossbauer pip), it is the basis of Huang-Rhys factors, and it appears elsewhere in condensed matter physics.

We are interested in this energy exchange mechanism because it has the potential to lead to anomalously large energy transfer. The total energy transfer ΔE is[89]

$$\Delta E = N\hbar\delta\omega$$

where N is the number of phonons present and where $\delta\omega$ is the phonon mode frequency shift. In the case of vacancy impurity phonon modes occurring in a phonon band gap, and separated by a band gap, the frequency shift can be a few meV. Either through the development of a phonon laser, or through stimulated Brillouin scattering, the number of phonons N can be made to be very large. An total energy shift greater than a few eV would be considered to be anomalous. The effect would be observable through the detection of fast ions or electrons produced at very high rates if the anomalous energy transfer process becomes allowed.

One approach to developing a large modal phonon density N is to generate an optical phonon laser. Phonon lasers have been demonstrated previously

---

[88] S. Kaushik and P.L. Hagelstein, "A Mixed Valence Model for Second Order Mixing of Neutron Orbitals in a Lattice," *Bull. Am. Phys. Soc.* 40: 317 (1995); P.L. Hagelstein and S. Kaushik, "Possibility of Neutron Hopping in Crystalline Silicon," submitted to *Phys. Rev. B.*

[89] P.L. Hagelstein, "Possible Mossbauer Effect in Neutron Capture," *Hyperfine Interact.* 92: 1059 (1994); P.L. Hagelstein, "Lattice-Induced Atomic and Nuclear Reactions," *Fusion Tech.* 26: 491 (1994).

at frequencies up to 0.87 THz. One of the most interesting demonstrations came about through the optical pumping of Cr ions in ruby by Hu (1980),[90] in which saturation of the phonon laser was claimed. To demonstrate anomalous energy transfer, phonon lasing of optical phonons may be required, which implies the development of phonon lasers at frequencies higher by factors of 5-20. Our application requires the use of materials with a phonon band gap, and an optical pumping scheme implies the use of a transparent crystal. This could be accomplished in LiH, or other transparent hydrides.

One potential difficulty associated with the proposed anomalous energy transfer mechanism discussed above concerns phonon loss. At low temperature, the lifetimes of phonons tend to be relatively long, and may be measured in units of a thousand cycles of oscillation. At room temperature or higher, the loss is much greater (the lifetime can be on the order of ten cycles), and it may be problematic to arrange for a coherent motion of a large number of atoms. This effect would rather drastically limit the maximum total energy transfer possible. However, if phonon gain is present, then the effect of phonon loss can be countered, and a large energy transfer may again be possible. Phonon gain may be more important in this problem than simply giving a large N.

We have recently considered exothermic desorption in metal hydrides as a candidate for driving surface phonon gain at high frequency.[91] A Hamiltonian that is appropriate for a metal hydride and gas system is:

$$\hat{H} = \hat{H}_{MeH} + \hat{H}_{ph} + \hat{H}_{gas} + \hat{H}_{int}$$

Hydrogen that is inside the metal is described by $\hat{H}_{MeH}$, which is of the form

$$\hat{H}_{HeH} = \sum_i \varepsilon_i \hat{b}_i^\dagger \hat{b}_i + \sum_{i,j} t_{ij} \hat{b}_i^\dagger \hat{b}_j$$

This includes the internal energy and hydrogen diffusion. Hydrogen molecules in the gas at low pressure are described by

$$\hat{H}_{gas} = \sum_k \varepsilon_k \hat{c}_k^\dagger \hat{c}_k$$

which includes the binding and kinetic energy. The phonons are assumed to be harmonic

$$\hat{H}_{ph} = \sum_{q\sigma} \hbar\omega_{q\sigma} \hat{a}_{q\sigma}^\dagger \hat{a}_{q\sigma}$$

Hydrogen in the metal can desorb to make molecular hydrogen; this is described by

$$\hat{H}_{int} = \sum_i \sum_k \left[V_{ijk}(\hat{a}) \hat{c}_k^\dagger \hat{b}_i \hat{b}_j + V_{ijk}^*(\hat{a}) \hat{b}_i^\dagger \hat{b}_j^\dagger \hat{c}_k \right]$$

This model is a generalization of the model of Gortel and coworkers.[92]

In the event that the desorption is exothermic (see figure 14), and if the interaction potential V is expanded to first order in the phonon operators $\hat{a}$, then the resulting model is equivalent to models used to describe lasers. The molecular hydrogen is not stable at the metal surface, which guarantees a population inversion whenever the ambient gas pressure is below the equilibrium pressure. As a phonon laser, this system is the analog of the optical excimer laser.

---

90 P. Hu, "Stimulated Emission of 29 cm $^{-1}$ Phonons in Ruby," *Phys. Rev. Lett.* 44: 417 (1980).

91 P.L. Hagelstein, "Lattice-Induced Atomic and Nuclear Reactions," *Fusion Tech.* 26: 491 (1994); P.L. Hagelstein, "Proposed Novel Optical Phonon Laser Pumped by Exothermic Desorption," *Bull. Am. Phys. Soc.* 40: 808 (1995).

92 Z.W. Gortel, H.J. Kreutzer, and D. Spaner, "Quantum Statistical Theory of Flash Desorption," *J. Chem. Phys.* 72: 234 (1980).

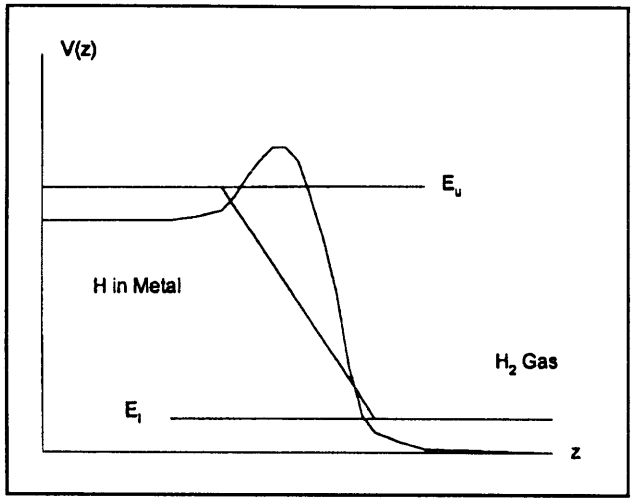

Figure 14. Schematic of potential for exothermic desorption.

Many metal hydrides become exothermic desorbers at high loading. For example, PdH is an endothermic desorber below a loading of about 0.9, and is an exothermic desorber at higher loadings. This is illustrated below in figure 15.

Because the theoretical gain for this system will be very high when gain exceeds loss, this phonon laser will be limited by the reaction kinetics and hydrogen diffusion. The gain criterion can be established immediately from the condition that the number of phonons generated must exceed the number of phonons destroyed per unit time. Assuming a highly excited surface phonon mode, we find the condition

$$\bar{n} J_{des} A > \frac{N}{\tau}$$

where J_{des} is the desorption flux, $\bar{n}$ is the mean number of phonons generated per desorption event, A is the area of the phonon mode, τ is the phonon lifetime, and N is the number of phonons in the mode (which must be on the order of 1 per atom at the surface in order to dominate over thermal effects). In metal hydrides at room temperature, the losses are very great, and phonon lifetime is on the order of 1 ps.

Consequently, the desorption flux must be very large. A desorption flux in the neighborhood of 10^{28} cm^2/sec appears to be the minimum flux required to produce optical phonon gain. This is not a sustainable flux, as it is impossible to develop an equivalent inward flux. Moreover, it cannot even be sustained by ordinary diffusion mechanisms.

We know that palladium can be loaded into the exothermic regime by either electrochemical or by ion bombardment techniques. In the electrochemical experiments, this is accomplished by developing a blocking layer that passes incoming ions, but blocks the outward gas flow. If this blocking layer were removed transiently on a very short (ns) timescale, then unhindered desorption would occur explosively. During such an explosive desorption event, a large desorption flux will be developed—whether it is sufficiently great to drive an optical phonon laser is presently unknown. A mechanism that causes hydrogen near the surface to be forced out at very high rates is required for large coherent phonon fields to build up.

In the case of impurity (for example, vacancy) optical phonon modes, the density of impurities is lower, and consequently the required desorption flux is lower by the dilution factor. In this case, desorption fluxes in the range of 10^{25}-10^{26} H_2/cm^2 sec are required, which is sustainable over nanosecond time-scales.

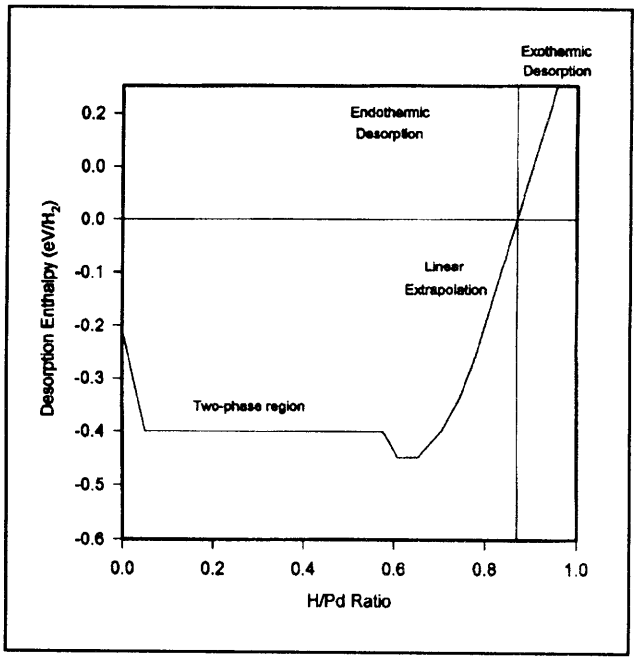

Figure 15. Relative internal potential energy for hydrogen in Pd as a function of loading.